Investigating the Adsorption and Transport of Water in MFI Zeolite Pores for Water Desalination

by

Thomas Humplik

B.S., Materials Science and Engineering (2008)

Lehigh University

Submitted to the Department of Mechanical Engineering in

Partial Fulfillment of the Requirements for the

Degree of Master of Science in Mechanical Engineering

at the

Massachusetts Institute of Technology

August 2010

[September 2010]

Signature of Author: .....

Department of Mechanical Engineering
August 26, 2010

Certified by: .....

Evelyn N. Wang
Assistant Professor of Mechanical Engineering
Thesis Supervisor

Accepted by: .....

David E. Hardt
Chairman, Department Committee on Graduate Theses

Investigating the Adsorption and Transport of Water in MFI Zeolite Pores for Water Desalination

by

Thomas Humplik

Submitted to the Department of Mechanical Engineering on August 26th, 2010,

in Partial Fulfillment of the Requirements for the Degree of Master of Science

Abstract

The permeability of reverse osmosis membranes is limited by the diffusive transport of water across a non-porous polyamide active layer. Alternatively, fabricating a microporous active layer capable of rejecting salt ions while allowing for water transport would increase the permeability while maintaining high salt rejection. Zeolites provide a model porous network which is capable of performing this type of molecular sieve separation. However, a lack of understanding of the mechanisms that govern transport within the zeolite pore network as well as an insufficient control of membrane synthesis has limited the performance of past zeolite-based membranes.

In this thesis, we seek to understand the mechanisms of water adsorption and transport in MFI-type zeolite pores through experimentation. Water adsorption on the surface and inside of the pore network was characterized by thermogravimetric analysis for varying Si/Al ratio zeolites. We estimated that the pore volume filled is ~71% for a 23 Si/Al ratio MFI zeolite, ~25% for an 80 Si/Al ratio MFI zeolite, and 0% for an infinite Si/Al ratio MFI zeolite. In addition, we characterized the transport of water into the MFI zeolite pore network by applying an increasing hydraulic pressure and measuring the change in volumetric displacement. We were able to corroborate the adsorbed pore volume from the TGA experiments and estimated that the pore volume filled was ~72% for a 23 Si/Al ratio MFI zeolite and ~34% for an 80 Si/Al ratio MFI zeolite. We also observed that the volumetric infiltration rate did not have an effect on the infiltration characteristics, which is distinctly different from continuum hydrodynamic behavior.

Future work will focus on testing the water permeation and salt rejection of these types of zeolites. We have made significant progress in the fabrication of defect-free zeolite membranes. We also plan on investigating the adsorption and transport of water in MFI zeolite pores by using molecular dynamics simulations.

Thesis Supervisor: Evelyn N. Wang

Title: Assistant Professor, Mechanical Engineering

Acknowledgements

I would like to graciously thank my advisor, Professor Evelyn Wang, for her care and guidance over the past two years. She has always respected my ideas, even if they sounded completely bizarre. I would not have been able to achieve the work in this thesis without her help and support.

I would also like to express gratitude to my peers in the Device Research Lab who have sat through my presentations and yet still had enough energy to provide me with thought provoking feedback. I would like to especially thank Dr. Shalabh Maroo, Dr. Ryan Enright, Batya Fellman and Jeremy Cho for helpful discussions during our sub-group meetings. I would also like to thank Yoshio Perez for all of his help with machining and troubleshooting my pressure infiltration vessel. My friends outside of MIT also deserve a great deal of my thanks for always being able to make me laugh and helping me momentarily forget my research setbacks.

Finally, I would like to thank my family. Without their unwavering support, I would not have been able to accomplish this dream of mine. Thank you for everything you have done.

Contents

Table of Contents

1. MOTIVATION AND BACKGROUND **12**

1.1 MOTIVATION 12

1.2 BACKGROUND 13

1.3 THESIS OBJECTIVES AND OUTLINE 19

2. SYNTHESIS AND CHARACTERIZATION OF MFI ZEOLITES **21**

2.1 ZEOLITE SYNTHESIS 21

2.2 ZEOLITE CHARACTERIZATION 23

2.3 SUMMARY 33

3. WATER ADSORPTION STUDIES **34**

3.1 PAST RESEARCH 34

3.2 EXPERIMENTAL PROCEDURE 37

3.3 EXPERIMENTAL RESULTS AND DISCUSSION 38

3.4 SUMMARY 45

4. PRESSURE INFILTRATION STUDIES **47**

4.1 PAST RESEARCH 47

4.2 EXPERIMENTAL SETUP 51

4.3 EXPERIMENTAL RESULTS AND DISCUSSIONS 53

4.4 SUMMARY 57

5. DEFECT-FREE MEMBRANE FABRICATION **59**

5.1 FABRICATION BACKGROUND AND DETAILS 59

5.2 SUMMARY 65

6. CONCLUSIONS AND FUTURE WORK **66**

6.1 FUTURE WORK 67

7. APPENDIX 1 **69**

7.1 SILICON/GLASS CLEAN PROCESS 69

7.2 PEI SPIN COATING 69

8. BIBLIOGRAPHY **71**

List of Figures

Figure 1. (a) Double five-ring SBU for MFI zeolite (b) Pentasil structure built from SBU (c) Skelatil diagram of MFI structure with pentasil group shaded for emphasis [22]. 14
Figure 2. Schematic of the intersecting pore structure of the MFI-type zeolite. 15
Figure 3. (a) Schematic of the system used by Murad and Lin [27]. (b) Enhanced schmatic showing the ZK-4 structure as well as water solutions. (c) Density plots of water, Na^+ and Cl^- with respect to the x-direction in the schematic. 16
Figure 4. (a) Cross sectional view of MFI zeolite RO membrane [29]. (b) Schematic of intercrystal pores which occur at the grain boundary of zeolite crystals 17
Figure 5. (a) Schematic of interfacially embedded zeolite/polyaimde membrane. (b) TEM image of cross section of membrane [30]. 18
Figure 6. Opened autoclave from Parr, Inc. with all associated parts. 21
Figure 7. Schematic of rotation device to synthesize uniformly shaped zeolite synthesis. 22
Figure 8. (a) Schematic of a basic XRD setup [34]. (b) Diffraction of x-rays showing how the angle is determined [21]. 24
Figure 9. X-ray diffraction pattern for Silicalite-I zeolites (in red) compared with the known diffraction peaks for MFI-type zeolites (blue) 25
Figure 10. Compiled XRD data for various MFI-type zeolites. Note that the Si/Al ratio has no effect on the long-scale structure of the zeolite. 25
Figure 11. Schematic of experimental setup used for XPS analysis [36] 26
Figure 12. XPS analysis of synthesized ZSM-5. The relative intensities for the (a) silicon and (b) aluminum are shown. 27
Figure 13. IUPAC classification for gas adsorption isotherms [37] 28
Figure 14. Schematic of typical gas adsorption analysis setup [37] 29
Figure 15. (a) Silicate-I zeolites on Si synthesized at 150 °C for 7 hours without rotation. (b) Magnified view of the zeolites displayed in (a) 30
Figure 16. (a) Silicalite-I zeolites synthesized at 180 °C for 5 hours with no rotation. (b) ZSM-5 (Si/Al - 23) zeolites obtained from Zeolyst, Inc. (c) Silicalite-I zeolites synthesized under rotation at 150 °C for 24 hours. (d) Oriented layer of zeolites on Si synthesized under rotation at 150 °C for 5 hours. 31
Figure 17. Sorption capacity of mordenite plotted against the Si/Al ratio. The line corresponds to the sorption capacity of 4 water molecules per aluminum site [43]. 34
Figure 18. Plot of % weight loss (x-axis) from TGA *versus* % alumina content (y-axis). Adapted from [44] 35
Figure 19. Schematic of zeolite pore structure and the location of the Al defects. 36
Figure 20. (a) Image of TGA and MS used for experiments (b) Close up view of sample pan being loaded into the furnace. 37
Figure 21. Derivative weight loss as a function of temperature for MFI 23 before heat treatment. The ion current associated with water is shown in blue. 39
Figure 22. Derivative weight loss as a function of temperature for MFI 23 after heat treatment. 40
Figure 23. Schematic of possible state of adsorbed water on surface of the zeolite after the heat treatment. 41
Figure 24. Derivative weight *versus* temperature for MFI 80 (in red) and MFI 23 (in black) before 42
Figure 25. Derivative weight *versus* temperature for MFI 80 (in red) and MFI 23 (in black) after 43
Figure 26. (a) Derivative weight *versus* temperature for MFI ∞ (in blue) before heat treatment (b) Derivative weight *versus* temperature for MFI ∞ (in blue) after heat treatment. 44
Figure 27. Normalized weight loss *versus* temperature for (a) MFI 23 (b) MFI 80 and(c) MFI ∞. Note that there is no difference before and after the heat treatment for MFI ∞, implying that water is never adsorbed in the pores. 45
Figure 28. Pressure-volume isotherm of the various "water-hydrophobic zeolite" systems. (1) zeolite-β (2) MFI (OH^- based) (3) MFI (F^- based) (4) Na-ZSM-5. Note that for (1), (A) symbolizes the step before intrusion and (B) the step after intrusion [55]. 47
Figure 29. Schematic of experimental setup used by Qiao *et al* [63] 49
Figure 30. Water sorption isotherms for the MFI 280 zeolites. The inset depicts what should occur if continuum approximations are applied [63] 49

Figure 31. (a) The formation of a single chain of water molecules in pore at ~50 MPa (top) and a double chain of water molecules at ~125 MPa (b) MD results of the pressure (solid symbol) and temperature (open symbol) as a function of the specific infiltration volume [63]. 50
Figure 32. General schematic of pressure vessel for infiltration experiments. 52
Figure 33.(a) Schematic of the two-piston pressure vessel used for infiltration experiments (b) Picture of the Instron 5582 with pressure vessel loaded into the apparatus. 53
Figure 34. The water infiltration isotherms for MFI 280 for varying infiltration rates. 54
Figure 35. Specific infiltration volume as a function of pressure for various MFI zeolites. 55
Figure 36. Schematic of ideal membrane for RO. The polymer must be water and salt impermeable. 59
Figure 37 (a) Oriented layer of MFI zeolites on a silicon support using mercapto-3 as a binding agent [64] (b) a-oriented MFI zeolites on a silicon support using 3-chloropropyltrimethoxysilane as a binding agent [65] 60
Figure 38. (a) Picture of a cleaned silicon wafer section (b) Zeolite powder deposited onto the surface of the cleaned silicon wafer (c) The final oriented zeolite layer on the silicon surface. 61
Figure 39. Single MFI zeolite (Si/Al - ∞) synthesized under rotation at 180 C for 12 hours; 62
Figure 40 b-oriented MFI zeolite on Si: (a) synthesis conditions: 180°C for 12 hours under rotation (b) 150 °C for 6 hours under rotation (c) 150 °C for 6 hours under rotation (d) 180 °C for 6 hours with no rotation. 63
Figure 41. (a) MFI zeolites deposited on a 100 nm Whatman Anodisc functionalized by a PEI adhesion layer. (b) Picture highlighting the low degree of surface coverage with this technique. 63

Chapter 1

1. Motivation and Background

1.1 MOTIVATION

The continuing increase in world population as well as the dwindling supply of useable fresh water has motivated researchers to find alternative methods to obtain potable water. Of these methods, desalination is the most widely used [1]. The combined desalination facilities around the world can produce upwards of 60 million cubic meters of fresh water per day. The seawater desalination capacity has increased at a rate of 29.6% over the last two years; however, even this increase has not been able to keep up with the growing demand for fresh water [2, 3]. It is estimated that by 2025, nearly two-thirds of the world's population will live under water-stressed conditions [3]. Therefore, the desalination capacity must continue to expand.

The main barrier preventing this expansion is that, in order to run these large-scale desalination facilities and create any sizeable amount of fresh water, a considerable monetary investment is required as well as access to a power grid. In addition to this, although current desalination systems operate near the theoretical minimum of energy required to separate water from seawater, the actual separation method is still largely inefficient [4]. Most of the increases in efficiency come from incorporating pressure recovery devices or optimizing system-level design [4].

The objective of this thesis is focused on increasing the permeability of reverse osmosis membranes and thereby increasing the separation efficiency. Current reverse osmosis membranes rely on the diffusive transport of water through a non-porous polymeric active layer. We aim to increase that permeability by using microporous materials that allow for water to transport through the membrane while rejecting the transport of salt ions, effectively creating a molecular sieve membrane for the desalination process. This thesis contributes in taking the first steps towards understand water transport and adsorption in sub-nanometer pores as well as synthesizing molecular sieve reverse osmosis membranes.

1.2 BACKGROUND

The reverse osmosis (RO) separation process applies the use of a semi-permeable membrane through which water is forced by an application of hydraulic pressure. The applied pressure ranges from 10 to 83 bar, depending on the salinity of the water and strength of the membranes [4]. This process removes dissolved salts and other organic molecules from the seawater solution to create fresh water. The method by which water transports through the membrane is known as solution-diffusion [5]. The membrane used for this process is a non-porous polymeric membrane composed of either cellulose acetate or an aromatic polyamide [6, 7]. Although salt ions can diffuse through these membranes, salt ion permeabilities are orders of magnitude lower than that of water so; therefore, a majority of salt and other organics is removed.

The total energy needed to desalinate seawater with RO depends on the salinity, flux, recovery rates and other operational conditions [4]. By incorporating energy recovery devices, current state of the art seawater RO desalination plants operate between 3 and 7 kWh per cubic meter of fresh water produced [2]. This is well below the energy required for thermal phase-change desalination systems such as multi-stage flash (MSF) or multi-effect distillation (MED) which ranges between 23 and 96 kWh/m^3 [8]. However, the average total capacity of RO is about a third of these phase-change desalination systems [8]. Most MSF plants operate by using the waste heat of power-producing plants, therefore, MSF plants are more numerous in the energy producing countries around the world [4], while RO is a stand-alone desalination technology and has become the primary method of desalination in western nations [2].

RO membranes rely on a thin (< 200 nm) polyamide active layer to separate the water from the seawater solution [2]. A macroporous polysulfone layer that is usually greater than 50 microns in thickness supports this active layer. The permeability of these polymeric RO membranes appears have reached its limit and most research now focuses on improving the fouling resistance, which is a major reason for the short lifetime of these membranes [2, 9-13]. However, there has been recent work on water transport through ordered nanoporous membranes composed of carbon nanotubes (CNTs) [14, 15] and aquaporins [16-18]. The permeability of these types membranes show orders of magnitude increase in flux over predicted values according to continuum hydrodynamics. The main challenge with these membranes has been that they have been unable to create a pore distribution that is capable of rejecting solvated salt

ions [19]. For example, the solvated size of a sodium ion is ~7.6 Å while the average diameter of the smallest CNT membranes is ~1.6 nm [14, 20]. Zeolite-type membranes offer a unique advantage over CNT and other nanofabricated membranes because the pore size can be synthesized to values smaller than that of a solvated salt ion whereas there is significant difficulty to produce this size distribution for CNT and other nanofabricated membranes.

Zeolites are a unique inorganic material that has a regular repeating pore structure with diameters ranging between 3 and 8 Å, depending on the zeolite. The basic building block of a zeolite is a TO_4 tetrahedron, where the T usually denotes either a silicon or an aluminum atom (in some cases, such as in aluminophosphate zeolites, the T denotes a phosphorus atom). In this thesis, we focused on the MFI-type zeolite, which is classified as an aluminosilicate zeolite and has the basic formula of $M_n[(Al)_n(Si)_{96-n}O_{192}].16H_2O$, where $n < 27$ and M denotes an non-framework, exchangeable cation (if present during synthesis). MFI zeolites have a framework density of 17.9 T atoms per 1000 $Å^3$ (this equates 1.78 g/cm^3) [21]. The structure of an MFI zeolite is composed of double five-ring secondary building units (SBUs), which can be assembled to create a pentasil structure that is shown in Figure 1.

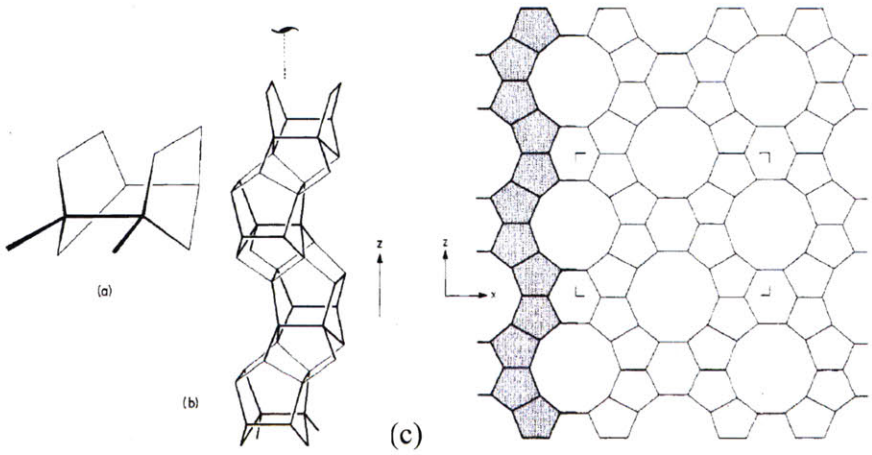

Figure 1. (a) Double five-ring SBU for MFI zeolite (b) Pentasil structure built from SBU (c) Skelatil diagram of MFI structure with pentasil group shaded for emphasis [22].

MFI zeolites can be either purely silicate (Silicalite-I) or alumino-silicate composite (ZSM-5), however, the crystal structure always remains unchanged. The structure is composed of a zigzag pore network running along [100] and an intersecting straight cylinder pore system that runs along [010]. The openings for the zigzag pore network is 5.1 Å x 5.5 Å while the opening for the straight cylinder pore network is slightly larger, 5.4 Å x 5.6 Å [22]. A schematic of the

crystal structure is shown in Figure 2. We chose the MFI zeolite for its pore size, which falls between the diameter of a solvated salt ion and the effective diameter of a water molecule (2.8 Å) [23].

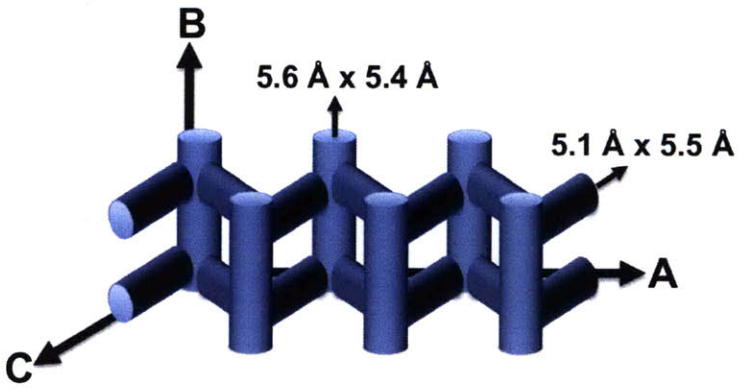

Figure 2. Schematic of the intersecting pore structure of the MFI-type zeolite.

MFI zeolites can be synthesized into a variety of sizes and morphologies [21]. The morphology can usually be controlled through the appropriate choice of structure directing agent (SDA) while the size is controlled by temperature and other synthesis conditions. The synthesis of MFI zeolites will be described in detail in the next chapter of this thesis.

Although the pore size seems to be appropriate, the question remains whether zeolite pores can reject salt ions and still allow for water permeation through size exclusion effects alone? Considerable progress in gas separation membranes showed that zeolite pores could in fact act as a molecular sieve [24-26]. However, water and ion transport through zeolite pores is different because of the strength of van der Waals interactions and electrostatic forces between the water molecules, ions and pore surface. Murad and Lin investigated this problem using molecular dynamic (MD) simulations. They used a ZK-4 zeolite (4.4 Å pores), which separated a fresh water bath from a simulated salt-water solution, as depicted in Figure 3. Since a concentration gradient existed between the salt water and the fresh water, a chemical potential should drive the ions across the pore and into the fresh water. However, Murad and Lin never observed the ions permeate through the zeolite structure (Figure 3c). They speculated that this was because of the increased diameter of the salt ions in relation to the zeolite pore. Also, they hypothesized that the large desolvation energies required to decrease the size of the solvated salt ion also aided in the salt rejection.

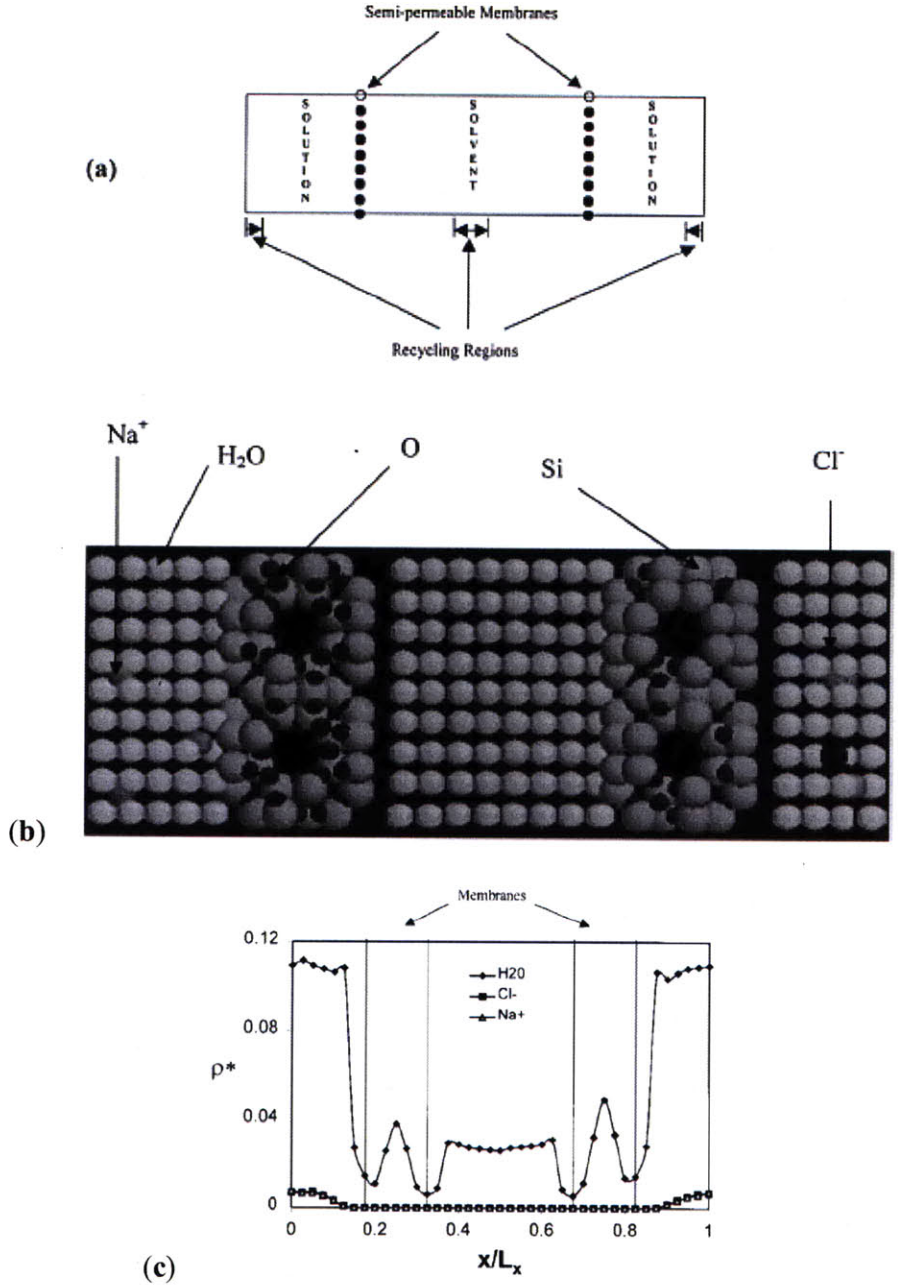

Figure 3. (a) Schematic of the system used by Murad and Lin [27]. (b) Enhanced schematic showing the ZK-4 structure as well as water solutions. (c) Density plots of water, Na^+ and Cl^- with respect to the x-direction in the schematic.

Therefore, the simulations by Murad and Lin showed that zeolite pores can reject salt ions while allowing for water transport. Li *et al.* used this as motivation to create RO membranes strictly from zeolites [28]. They used MFI-type zeolites that were grown directly onto a porous

alumina support (this membrane synthesis is known as the direct growth method). The membrane thickness was approximately 3 μm. An SEM of the cross section of a typical direct growth membrane is shown in Figure 4a.

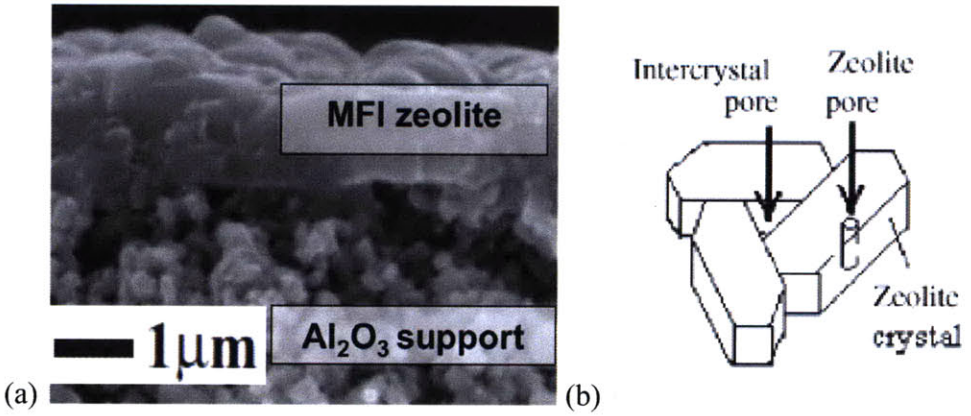

Figure 4. (a) Cross sectional view of MFI zeolite RO membrane [29]. (b) Schematic of intercrystal pores that occur at the grain boundary of zeolite crystals.

The fabricated MFI zeolite membrane, however, did not exhibit the salt rejection that Murad and Lin had predicted. While it was expected that the water permeability of the membrane would be low because of the thickness of the membrane and the hydrophobicity of the zeolite, it was surprising that the salt rejection was only ~58% for ~0.5 M NaCl solution. The low salt rejection was attributed to the intercrystalline defects that form at the grain boundaries of the zeolite crystals. These intercrystalline defects create gaps that range in size between 1 and 10 nm (highlighted in Figure 4b). Therefore, these gaps create pathways for water and salt ions to flow around the zeolite, rendering the sieving properties of the zeolite ineffective. Salt rejection was higher when the salinity of the water decreased to values less than 0.1 M. This results suggests that an electrokinetic effect arising from the surface charge on the zeolite[1] in the intercrystal pores was restricting the passage of ions through the membrane. Li *et al.* attempted to increase the permeability by decreasing the Si/Al ratio of the zeolite in later work. While this did have the desired outcome, as the permeability increased by an order of magnitude, the salt rejection was still low for high concentration salt water (0.3M NaCl). A summary of their results is shown in Table 1. Overall, the membrane still exhibited permeabilities that were at least an order of magnitude lower than that of polymeric RO membranes.

[1] This is most likely due to the high concentration of silanol (Si-O-H) groups at the surface of the zeolite crystal

Table 1. Compiled permeability and salt rejection results from direct growth zeolite RO membranes.

Membrane	Permeability (m/Pa•s)	Solution (NaCl)	Salt Rejection	Source
MFI (Si/Al - ∞)	$1.36x10^{-14}$	0.1 M	76%	[28]
MFI (Si/Al - ∞)	$8.05x10^{-14}$	~0.5 M	58%	[28]
ZSM-5 (Si/Al - 37)	$1.14x10^{-13}$	0.1 M	98%	[29]
ZSM-5 (Si/Al - 37)	$8.5x10^{-13}$	0.3 M	~93%	[29]

Another method of incorporating zeolites into RO membranes is to interface the zeolites within a state-of-the-art RO membrane. Jeong *et al.* used LTA type zeolites (same class as those studied by Murad and Lin) and interfacially embedded them into the polyamide active layer. They assumed that the "super-hydrophilic, negatively charged, molecular sieve zeolite nanoparticles will provide preferential flow paths for water permeation while maintaining high solute rejection through combination of steric and Donnan exclusion [30]." A schematic and a TEM image of the membranes are presented in Figure 5.

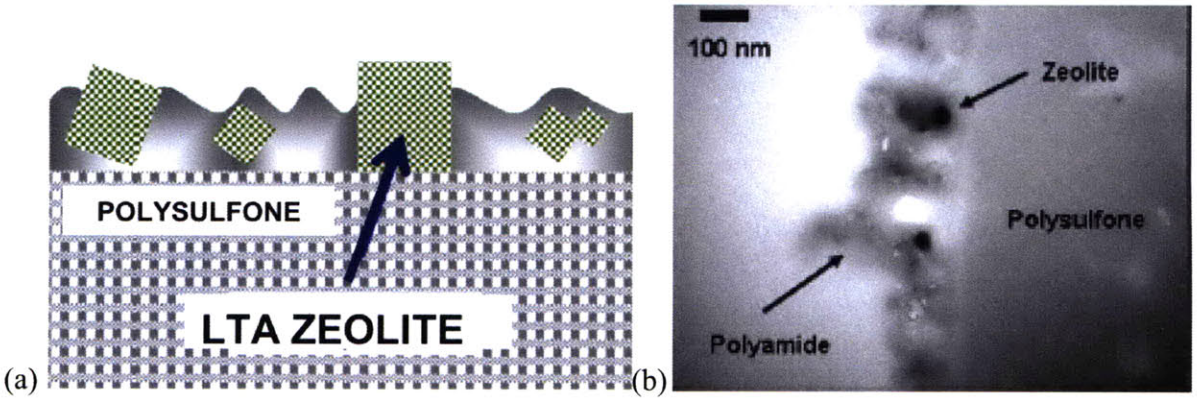

Figure 5. (a) Schematic of interfacially embedded zeolite/polyamide membrane. (b) TEM image of cross section of membrane [30].

Jeong *et al.* compared their synthesized membranes against synthesized non-zeolite loaded polyamide membranes and state-of-the-art RO membranes. While their results showed improvement in permeability over the non-loaded membranes synthesized in their lab, the permeability showed no improvement over when compared to the commercialized state-of-the-art RO membranes (shown in Table 2). Thus, the membranes again do not show the permeability increases required to increase the separation efficiency of RO systems.

Table 2. Compiled permeability and salt rejection values for embedded zeolite RO membranes [30].

Membrane	Type	Permeability (m/Pa•s)	Salt Rejection
TFC	No embedded zeolites	2.1×10^{-12}	93.20%
TFN-400	40 wt% zeolite loaded	3.8×10^{-12}	93.90%
XLE	Commercial	1.68×10^{-11}	93%

Both types of membranes share one specific problem: water molecules and ions are allowed to transport around the zeolite crystal. Therefore, it is difficult to determine the role of the zeolite in the transport of water and rejection of salt. In order to understand the role of zeolites and to determine whether or not they will provide any benefit to RO, the fundamental transport and adsorption mechanisms across single crystal zeolite particles must be investigated. In addition, better control of membrane fabrication is required so that transport across the zeolite pores can be studied.

1.3 THESIS OBJECTIVES AND OUTLINE

The structure and pore size of zeolites promise to increase the permeability and salt rejection over commercial polymeric RO membranes for seawater desalination. MD simulations have shown that zeolite pores can perfectly reject solvated salt ions while allowing for water to permeate through. However, past experimental results using zeolites for RO have yet to realize this potential. A problem with the experimental membranes is that they allow for water and salt transport around the zeolite crystal. Therefore, the molecular sieving capability of the zeolite is not being appropriately applied. From past experiments, it is clear that the water transport and

adsorption mechanisms for zeolites used as a water desalination membrane are not fully understood. The objective of this thesis is to begin to fundamentally understand these mechanisms and apply them to create a more efficient zeolite-based RO membrane. To accomplish this, we combine thermogravimetric analysis of water adsorption on MFI-type zeolites with studies investigating the transport of water in single crystal zeolites. We also describe the process to synthesize defect free zeolite membranes that limit the transport of water and salt ions to the zeolite pores. Since the size of the zeolite pores is smaller than 1 nm, it is inappropriate to apply intuitions and relations derived from continuum analysis for this work. Thus, the findings of this work not only impacts RO membrane design, but also provides insight into the mechanisms that govern transport on the sub-nanometer scale. The structure of this thesis is outlined below:

In Chapter 1, we outline the motivation for this work as well as provide a review of the zeolite structure and the past research of zeolites used for RO desalination.

In Chapter 2, we describe in detail the synthesis methods to create MFI-type zeolites with a varying Si/Al ratio. We also describe the characterization techniques we used to determine the structure and material properties of the synthesized zeolites.

In Chapter 3, we describe the thermogravimetric analysis and the methods we applied to determine the amount of water that was adsorbed inside the MFI-type zeolites.

In Chapter 4, we explain the motivation for the pressure infiltration experiments, the setup for the experiments and the findings of these experiments.

In Chapter 5, we introduce a methodology for creating defect free zeolite membranes that should limit the transport of water and ions to the zeolite pores.

In Chapter 6, we conclude the thesis and describe the major findings in this work. We also describe the future work we have planned to further investigate transport through sub-nanometer zeolite pores.

Chapter 2

2. Synthesis and Characterization of MFI Zeolites

2.1 ZEOLITE SYNTHESIS

Synthesizing natural zeolites take thousands of years, and therefore cannot be reproduced in a laboratory setting. However, synthetic zeolites can be created with correct chemicals and conditions. Barrer and coworkers in the 1940s were the first group that was able to synthesize zeolites using hydrothermal synthesis, which is the same technique we use to create MFI zeolites [31]. Hydrothermal synthesis entails using conditions of high temperature (> 100 °C) and high pressure (> 10 bar) in a closed system. To achieve this, we use a stainless steel autoclave (Parr, Inc) with a PTFE inner liner (also known as a cup), shown in Figure 6.

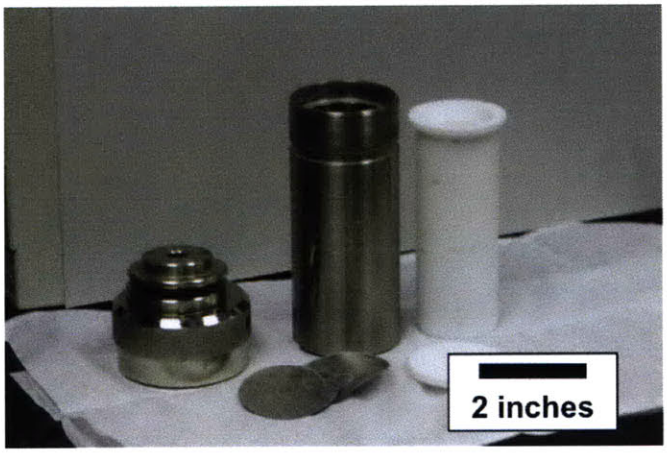

Figure 6. Opened autoclave from Parr, Inc. with all associated parts.

To synthesize Silicalite-I zeolites, three ingredients are needed: a structure directing agent (SDA), a silica source, and water. If ZSM-5 zeolites are desired, a source of alumina must also be added during synthesis. First, we will describe the synthesis of Silicalite-I zeolites, according to the procedure of Lai *et al.* [29].

A monomer-tetrapropylammonium hydroxide (TPAOH) is used as the structure-directing agent. This SDA is known to produce thin, disc-shaped MFI zeolites. A variety of shapes and sizes can be synthesized by varying composition of the SDA, silica source and water. For chemicals, we used TPAOH (1M in H_2O, Aldrich), tetraethylothrosilicate (TEOS, 98%, Sigma),

and deionized H_2O (Class 2, VWR). All chemicals were used as received. To produce ~500 nm ± 100 nm diameter particles with an average thickness of ~200 nm ± 50 nm, a molar ratio of 5 TEOS:1 TPAOH: 500 H_2O is used (4.98 g TPAOH, 5.00 g TEOS, 39.2g H_2O). TPAOH and TEOS are first mixed in a beaker with a magnetic stirring rod while water is slowly added. The solution is left to age, stirring at ~ 200 RPM for 12 hours. After the aging process, the solution is filtered using 500 nm filter paper (Parr, Inc) using a vacuum filtration apparatus. The clear, filtered solution is then transferred to the PTFE cup inside of the autoclave and the autoclave is closed and tightened using a hook spanner. The autoclave is then placed inside of an oven at 150 °C and left stagnant for 6 hours. After 6 hours, the autoclave is removed from the oven and quenched to room temperature in water. The solution is extracted from the PFTE cup and poured into a 45 mL Corning© centrifuge tube. The resulting solution is centrifuged at 8000 RPM for 10 minutes to separate the zeolites from the synthesis solution. The separated solution is poured from the tube and replaced with deionized water. The centrifugation steps are repeated three times to bring the pH of the solution to 8. The water/zeolite solution then is dried at 60 °C overnight in a watch glass. Since the SDA is still present in the pores at this point, a final heat treatment (known as calcination) of 550 °C for 6 hours (with 1 °C/min ramp rates) is needed to purge the pores. To produce 2 μm diameter particles with a uniform shape, a same procedure is used but with one major change. During synthesis, the solution must be rotated so that these large diameter zeolites with a uniform size distribution are created. To do this, we built a device that could rotate the autoclave while it is inside of the oven. A schematic of the rotation device is shown in Figure 7.

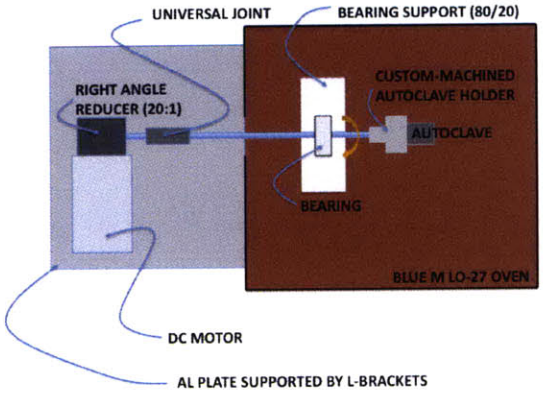

Figure 7. Schematic of rotation device to synthesize uniformly shaped zeolite synthesis.

The synthesis composition, time, and temperature remained the same as the previously described zeolite synthesis. Increasing the temperature of the synthesis can increase the size. For example, 5 μm Silicalite-I zeolites can be synthesized with the same composition when the temperature and time are 180 °C and 12 hours, respectively.

To change the silicon to aluminum (Si/Al) ratio of the zeolites, an alumina source must be added during the synthesis. The nomenclature of the zeolites changes from Silicalite-I to ZSM-5, however, the structure remains the same. To synthesize ZSM-5 zeolites with a varying Si/Al ratio, we referenced the procedure by Wang *et al.* [32]. First, we synthesized zeolites with a Si/Al ratio of ~50. The solution was prepared by mixing 0.016 g sodium hydroxide (anhydrous pellets, Aldrich), 22.3 mL of deionized H_2O (Class 2, VWR), 15 ml tetrapropylammonium hydroxide (TPAOH, 1 M in H_2O, Aldrich), 0.262 g aluminum isopropoxide [$Al(Pro)_3$, 98%, Sigma] and 14.2 ml tetraethylorthosilicate (TEOS, 98%, Sigma). The molar ratio of the solution was 0.3 NaOH : 0.5 Al2O3 : 50 SiO2 : 12 TPAOH : 1600 H2O. The solution was stirred with a magnetic stir bar in a glass beaker for 12 hours and then filtered with 500 nm filter paper (Parr, Inc) using a vacuum filtration device. The solution was transferred to a PTFE cup and sealed in an autoclave. The solution was heated in an oven at 140 °C from 4-6 hours under rotation. The rotation of the autoclave did not seem to have an effect on the size uniformity of the zeolites, as the zeolites produced were large (> 2 μm) aggregates. The solution was centrifuged using the same method as the Silicalite-I zeolites and dried at 80 °C in a watch glass. The resulting zeolites were calcined at 550 °C for 6 hours (with 1 °C/min ramp rates). To decrease the Si/Al ratio (*i.e.*, increase the amount of aluminum present in the zeolite), the same methodology was used, however, the amount of aluminum isopropoxide was increased to 0.437 g.

2.2 ZEOLITE CHARACTERIZATION

There are a variety of methods to characterize zeolites for any given application. In this section, we will focus on characterization techniques used to validate the synthesis recipes and procedures along with determining the size and pore volume of the zeolites that were created.

2.2.1 ZEOLITE STRUCTURE

X-ray diffraction (XRD) relies on the x-rays to determine the diffraction angles of a given structure. XRD can determine the long-range crystallinity of a given structure if the distances between the atom planes is on the same order of the x-ray radiation (~1-2 Å) [21]. Electrons and, to a lesser extent, neutrons can also be used, however, XRD is the most established technology. There are many types of XRD but we will focus on powder x-ray diffraction in this thesis since it will provide the overall structure of the synthesized particles (instead of the diffraction pattern of a single MFI zeolite which has already been establish with previous work [33]). A schematic of a typical X-ray diffractometer is shown in Figure 8 as well as a diagram of the diffraction fundamentals.

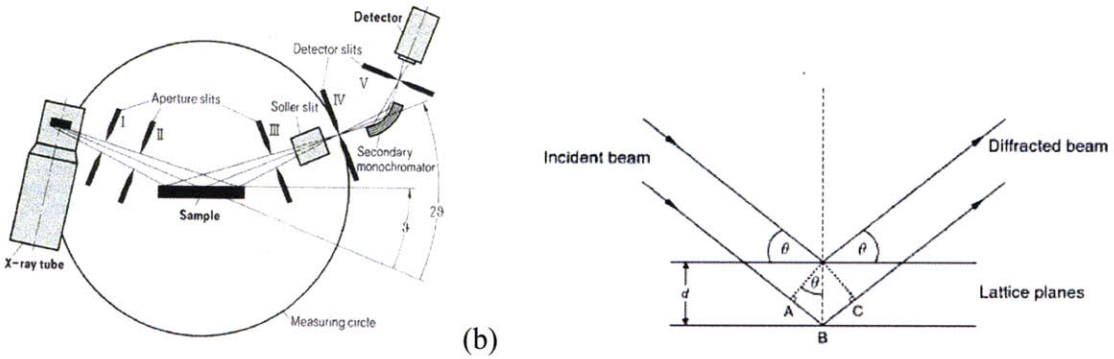

Figure 8. (a) Schematic of a basic XRD setup [34]. (b) Diffraction of x-rays showing how the angle is determined [21].

The distance between the lattice planes as well as the crystal structure can be found by using the well-known Bragg Law, shown in equation 1.

$$n\lambda = 2d\sin\theta \tag{1}$$

where λ is the wavelength of the incidence beam, n is a constant, d is the distance between the lattice planes, and θ is the diffraction angle. Diffraction peaks for structure characterizations are determined when n is equal to 1 [35].

To determine the structure of the zeolite, a sample of ~ 50 mg is loaded onto a sample holder and inserted into a XRD apparatus. For these experiments, we used a Phillips PANalytical X'PERT PRO diffractometer with a Ni-filtered Cu Kα (λ=0.15418 nm) incident radiation. A 0.04 soller slit along with a 1° fixed angle aperture slits are used. The step size was 0.0175 °, and

the counting time per step was 8 s. The XRD patterns Silicalite-I zeolites were found before and after the calcination process to determine the diffraction peaks of the TPAOH. Figure 9 shows the diffraction pattern for the calcined MFI samples as well as the known diffraction peaks of MFI-type zeolites.

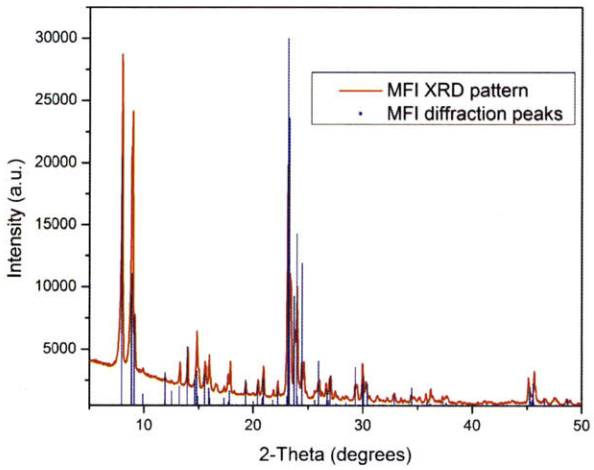

Figure 9. X-ray diffraction pattern for Silicalite-I zeolites (in red) compared with the known diffraction peaks for MFI-type zeolites (blue).

The XRD patterns were also determined for ZSM-5 zeolites and are shown in Figure 10. As expected, the diffraction data does not deviate from the previously measured and known MFI diffraction peaks.

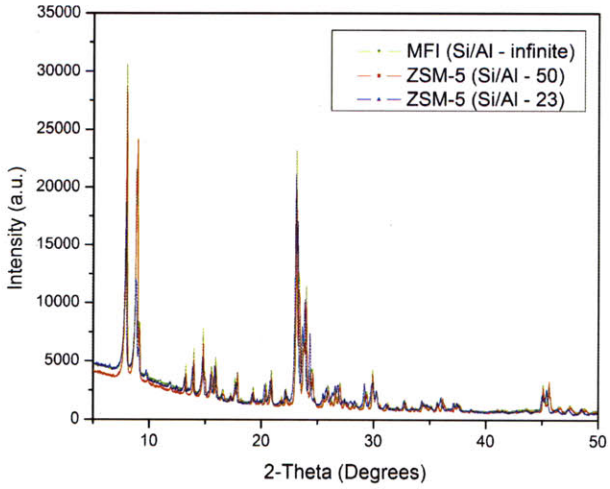

Figure 10. Compiled XRD data for various MFI-type zeolites. Note that the Si/Al ratio has no effect on the long-scale structure of the zeolite.

2.2.2 DETERMINING THE SI/AL RATIO

X-ray photoelectron spectroscopy (XPS) can be used to determine the Si/Al ratio of the zeolites. Although XPS is a surface analysis procedure (only penetrating ~5 nm) due to the short range of the photoelectrons that are excited, the XPS was performed over a wide spot size (>1 μm) so that an average Si/Al ratio could be determined. XPS relies on determining the energy of the reflected x-ray radiation and the change from its initial energy state. The change in energy can be quantitatively analyzed and matched to a specific chemical or electronic state of an element. Also, from the magnitude of x-ray reflection, an approximate chemical composition can be determined (in our case, the amount of silicon and aluminum in the zeolite). A schematic of an XPS analysis system is shown in Figure 11.

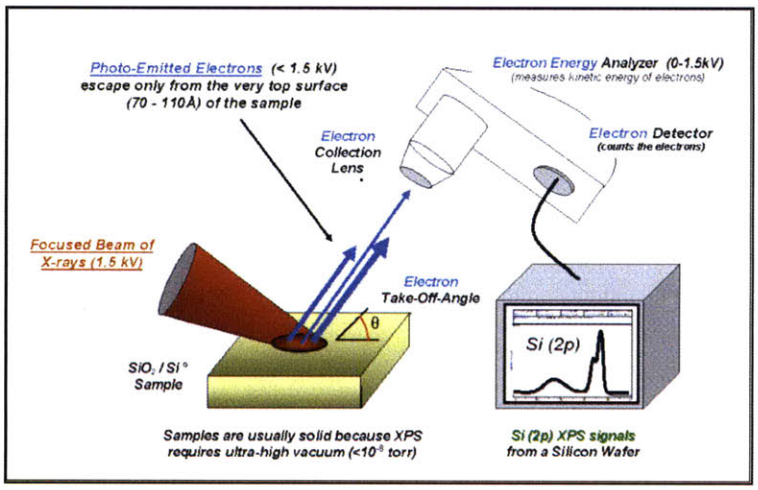

Figure 11. Schematic of experimental setup used for XPS analysis [36].

X-ray photoelectron spectroscopy was performed using a KRATOS Axis ultra electron spectrometer. The spectra were excited by the monochromatized Al KR source (1486.6 eV) and run at 15 kV and 10 mA. The Si/Al ratio was determined for a variety of zeolites. In Figure 12, an example of the data found by the XPS is shown. From this data, the Si/Al ratios can be estimated by taking the ratios of the relative intensities of the silicon (Figure 12a) and aluminum peaks (Figure 12b). The relative intensities are determined by finding the peak height of each curve.

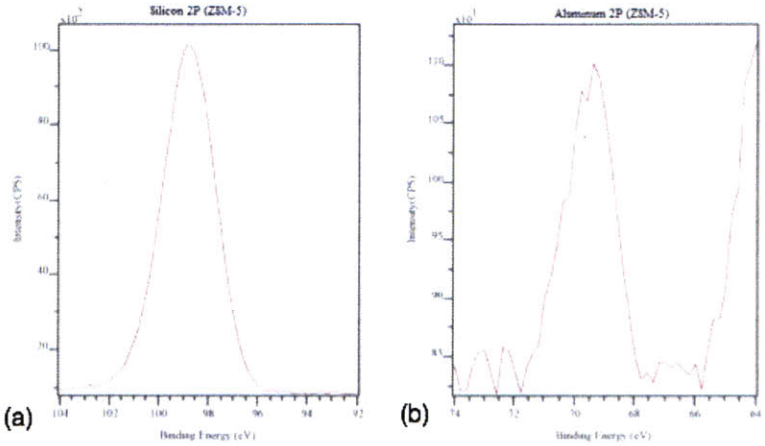

Figure 12. XPS analysis of synthesized ZSM-5. The relative intensities for the (a) silicon and (b) aluminum are shown.

A compiled list of XPS data is shown in Table 3. There is deviation from the projected Si/Al ratios, however this is not entirely unexpected. There is some human error involved in measuring the quantities of chemicals used for zeolite synthesis. As long as the Si/Al values do not deviate significantly from the predicted values (>10), the measured Si/Al ratio is acceptable.

Table 3. Compiled XPS data for synthesized zeolites.

Zeolite	Predicted	XPS
ZSM-5 / 25	25	28 ± 6
ZSM-5 / 50	50	47 ± 3
Silicalite-I	∞	>1000

2.2.3 PORE VOLUME ANALYSIS

The surface area and pore volume of a given material can be determined by studying the adsorption of a gas (*i.e.,* nitrogen or argon) as a function of pressure, more commonly known as determining the gas physisosorption isotherm. In 1985, the International Union of Pure and Applied Chemistry (IUPAC) classified the known adsorption isotherms into six types of adsorptive behaviors [37]. Of these, the most common types of adsorption isotherms that zeolites exhibit are either type I or type IV isotherms, shown in Figure 13.

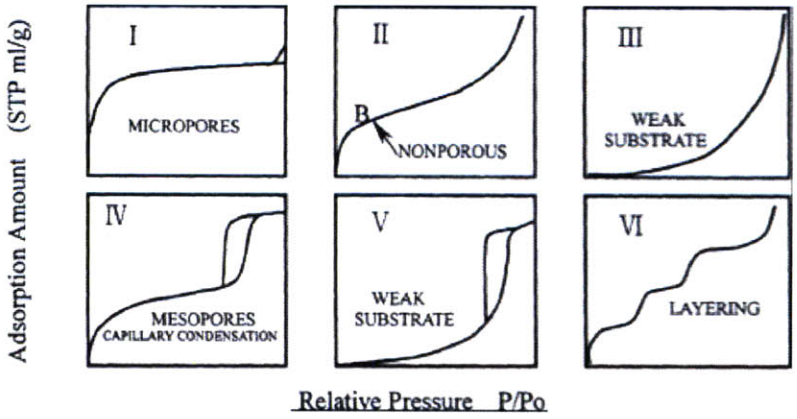

Figure 13. IUPAC classification for gas adsorption isotherms [37].

Gas adsorption in zeolites is complex and complete understanding of the kinetics and transport mechanisms has yet to be established, even though it has been studied for over thirty years [38]. The micropores[2] of zeolites tend to adsorb a significant amount of adsorbate in the low-pressure regime, however, the behavior is dependent on the adsorbate gas. Argon gas tends to exhibit a type I adsorption isotherm while nitrogen gas will exhibit a low pressure type IV adsorption isotherm in ZSM-5 type zeolites [39]. Although this behavior is still not fully understood, one theory suggests that the zeolites can undergo a small change in structure to accommodate itself to the adsorbate [40]. However, structural deviation alone may not account for the changes observed in the adsorption behavior [37].

For our experiments, we were seeking to quantify the total available pore volume of the zeolites we synthesized as well as the zeolites we commercially obtained from Zeolyst, Inc. We used a Micromeritics ASAP 2020 gas adsorption analyzer, which relies on measuring the changes in volume as a function of pressure to determine the adsorption isotherms. This type of gas adsorption analyzer has a typical working diagram shown in Figure 14.

[2] According to classic terminology, microporous materials are those with less than 2 nm pore diameters, although they are now common referred to as 'nanoporous' materials.

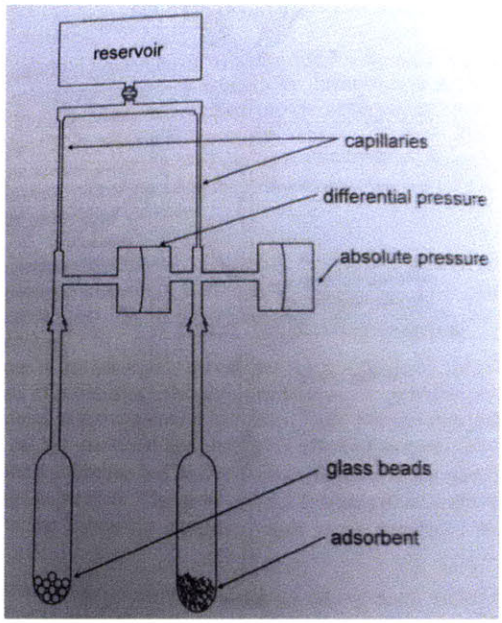

Figure 14. Schematic of typical gas adsorption analysis setup [37].

Nitrogen adsorption and desorption isotherms were measured at liquid nitrogen temperature and the pore volume was deduced by applying the B.E.T. equation[3] [41]. The typical isotherm obtained in our experiments shows the same behavior as previously reported [39]. In Table 4, we report the available pore volume for various MFI-type zeolites found by the 2020 gas adsorption analyzer as well as data reported in literature [40].

Table 4. Comparison of pore volumes attained by N2 adsorption with BET analysis of various Si/Al ratio zeolites.

Zeolite	Si/Al ratio	Pore Volume (cm^3/g)	Source
MFI 1	∞	0.1986	Synthesized
MFI 2	280	0.2009	Zeolyst, Inc
MFI 3	23	0.1954	Zeolyst, Inc
MFI 4	27 ± 6	0.2001	Synthesized
Silicalite-I	∞	0.19	Kenny and Sing [42]

[3] Although the B.E.T. equation is valid only for monolayer adsorption and seems to underestimate the total pore volume for zeolites, it is still openly used as a benchmark to estimate the pore volume.

Although our data shows slightly larger pore volumes, all data were within ~5% of the pore volume reported by Kenny and Sing [42].

2.2.4 CRYSTAL SIZE ANALYSIS

There are various ways to analyze the size of the crystals. Here, we will review the two that we used: Scanning election microscopy (SEM) and dynamic light scattering (DLS). Both methods have their benefits and should be used in conjunction with each other to obtain the best size analysis.

Scanning electron microscopy relies on detecting the scattering of electrons at a surface. In a typical thermionic SEM, a tungsten filament is energized through the application of high voltages to emit an electron beam. The beam is focused through a variety of condensing lens and the electron beam then interacts with the surface. Depending on the detector, electrons that scatter from the sample are recorded and an image is created from this data. SEMs are extremely useful because they can produce images well below the diffraction limit of visible light (~500 nm) and can also provide a level of depth to an image. Most SEMs today can produce images of artifacts below 10 nm in size . For our experiments, we use a Phillips XL30 Environmental Scanning Electron Microscope (ESEM), which is capable of viewing a conducting or non-conducting sample (although at lower resolution). Samples were coated with ~15 nm of gold deposited by evaporation to obtain higher image resolutions.

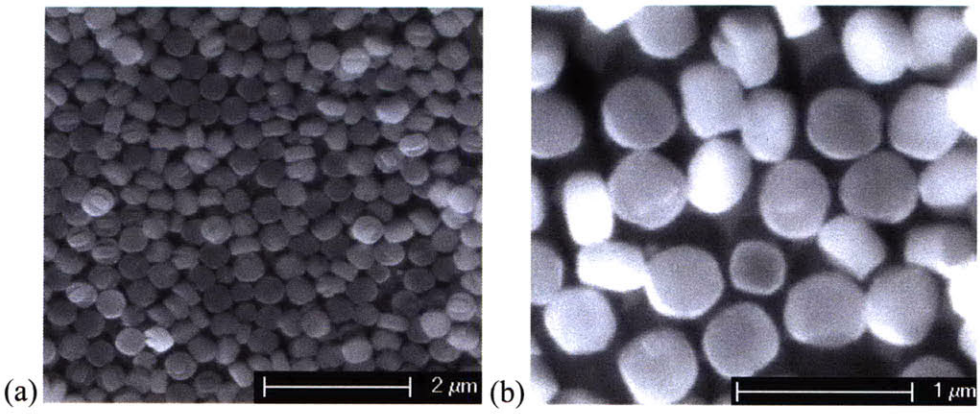

Figure 15. (a) Silicate-I zeolites on Si synthesized at 150 °C for 7 hours without rotation. (b) Magnified view of the zeolites displayed in (a).

The Silicalite-I zeolites in Figure 15 were synthesized without rotation. Although the size distribution appeared small at first, further analysis (Figure 15b) shows a large distribution in size, ranging from 400 nm to 600 nm in diameter. The SEM also revealed that some zeolites formed twins and therefore distorted the shape from a disc to a three-dimensional cross. Although an average size is tedious to quantify from SEM, a SEM helps in determining the crystal morphology as well as any other abnormalities that light scattering techniques cannot differentiate.

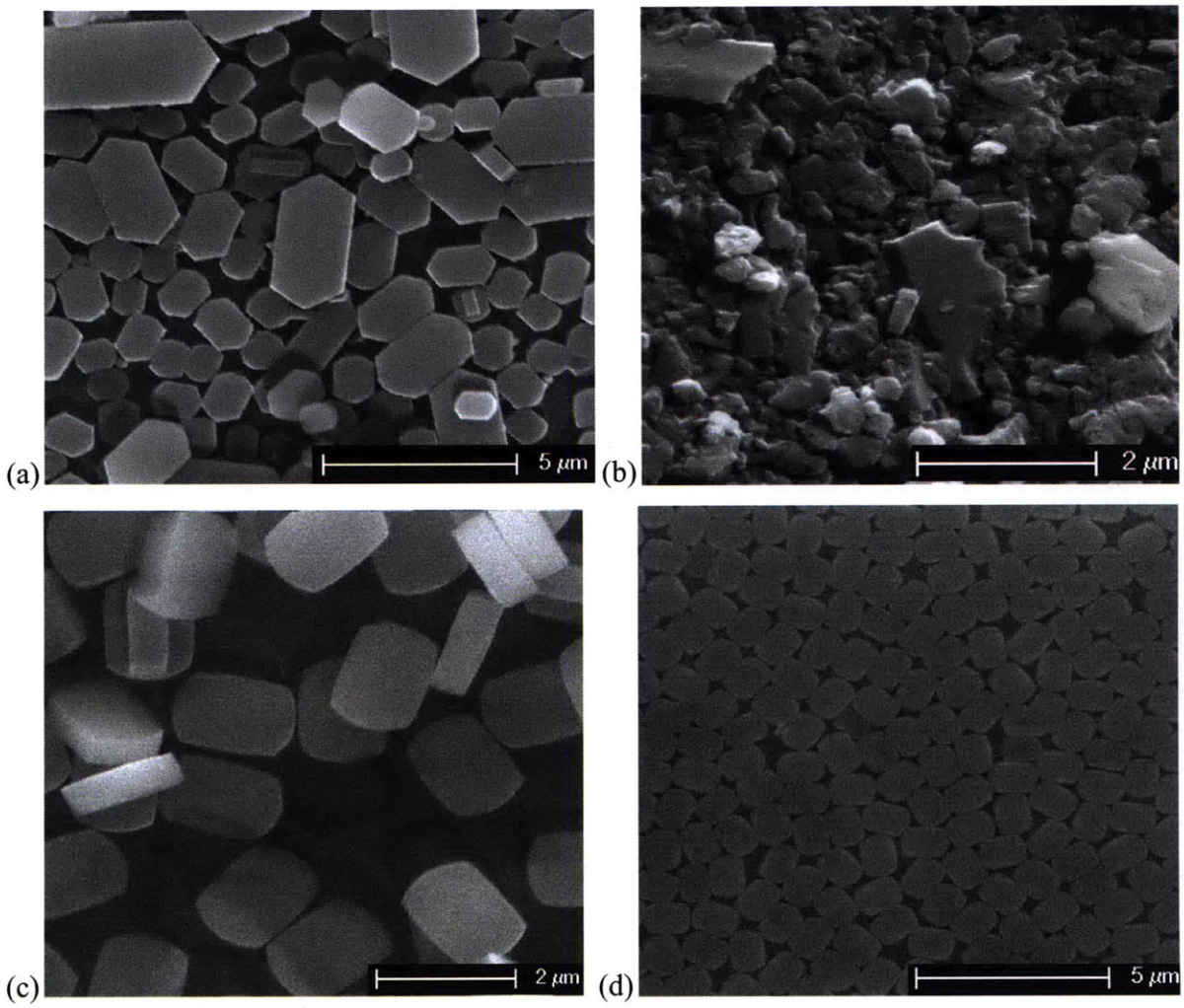

Figure 16. (a) Silicalite-I zeolites synthesized at 180 °C for 5 hours with no rotation. (b) ZSM-5 (Si/Al - 23) zeolites obtained from Zeolyst, Inc. (c) Silicalite-I zeolites synthesized under rotation at 150 °C for 24 hours. (d) Oriented layer of zeolites on Si synthesized under rotation at 150 °C for 5 hours.

Figure 16 shows the range of different size and shapes of zeolites that are possible by varying the temperature, condition, and synthesis time. These zeolites were either synthesized in the lab (Figure 16 a, c, d) or commercially obtained (Figure 16 b). Zeolites that were synthesized under rotation showed a size deviation of less than 50 nm. The zeolites obtained from Zeolyst, Inc. showed a non-uniform shape and a size deviation of over 1 μm. These zeolites were fabricated in a large-scale factory environment and were intended to be used as commercial adsorbents, therefore, crystal size and shape are not of great importance. These zeolites are helpful for adsorption studies and transport studies in that will be described in chapters 3 and 4, respectively.

The other method we used to characterize the size of the zeolite crystals was dynamic light scattering (DLS), a laser scattering method. To perform a DLS experiment, a solution of water and 'particles' was needed. The concentration of particles should be extremely low (< 20 mg/L) to avoid error in the data. The obvious advantage of this type of characterization is the speed; an average DLS experiment will take less than 5 minutes from start to finish whereas an SEM analysis will take a few hours. However, one needs to determine the density of the particles and pH of the solution prior to the experiment as these two factors weigh heavily in the analysis portion of the experiment. The DLS also provides a distribution of size for the crystals and can determine if there are two different length scales present in the solution, a task that is quite tedious to determine using traditional SEM techniques. The DLS is usually combined with a zeta potential analyzer which provides the possibility of determining the surface charge, which can be helpful to determine the charge effects for transport. The main disadvantage of the DLS is that the experiment relies on the Raleigh scattering of light off the particles. Therefore, the particles should be less than 500 nm in size and, more or less, uniform in diameter. Although we have used these experiments to characterize zeolite crystals that are larger than 500 nm in size and report these findings, we are not confident in the results that were obtained. In Table 5, we present the data obtained from the DLS experiments. Qualitatively, they validate the visual analysis performed using the SEM.

Table 5. Complied crystal size data found using DLS. Note references to SEM figures in previous section.

Zeolite	Si/Al ratio	Average Size (DLS)	Source	SEM
MFI 1	∞	0.48 ± 0.1 μm	Synthesized	Figure 9a
MFI 1a	∞	0.35 ± 0.1 μm	Synthesized	N/A
MFI 1b	∞	0.824 ± 0.6 μm	Synthesized	Figure 10d
MFI 2	280	1.85 ± 1.2 μm	Zeolyst, Inc	Figure 10b
MFI 3	23	2.35 ± 2.1 μm	Zeolyst, Inc	N/A

2.3 SUMMARY

In this chapter, we reviewed the procedure for synthesizing various MFI type zeolites using the hydrothermal synthesis technique. We also reviewed the basic principles behind the characterization techniques used and showed the results from the characterization experiments. Although these experiments are needed to determine the structure, size, and the Si/Al ratio of the zeolites, they do not show any information on the adsorption and transport of water in the zeolites. In the following chapters, we will elaborate on the experiments used to determine the transport and adsorption properties.

Chapter 3

3. Water Adsorption Studies

3.1 PAST RESEARCH

The effect of the Si/Al ratio on water adsorption in the MFI zeolite pore network has not been quantitatively studied. Although it is well known that increasing the Si/Al ratio of a zeolite increases hydrophobicity [21], the extent of research on the actual effect of the Si/Al on water adsorption has been limited. Chen was the first to hypothesize the role of defects in water adsorption [43]. Chen investigated synthetic mordenite-type zeolites and studied the adsorption of water vapor gravimetrically from pressures ranging from vacuum to saturation. From his data, Chen was able to see that each additional alumina site allowed for a coordination (or adsorption) of four water molecules. In Figure 17, Chen plots the final adsorption amount as a function of the Si/Al ratio recorded at 25 °C and at 12 mmHg of water. Although there is considerable scatter in the data, especially in the high Si/Al ratio regime, the trend is seemingly linear and follows a slope associated with four water molecules per Al atom in the framework. Chen does indicate that the linear trend no longer holds at lower Si/Al ratio (<10), possibly because the pores become saturated with water and can therefore not adsorb any more water.

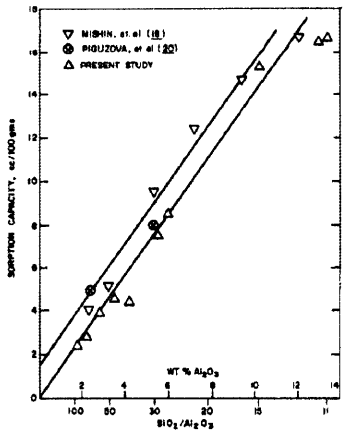

Figure 17. Sorption capacity of mordenite plotted against the Si/Al ratio. The line corresponds to the sorption capacity of 4 water molecules per aluminum site [43].

Hill and Seddon investigated the adsorption of water on H-ZSM-5 zeolites with varying Si/Al ratios using thermogravimetric analysis (also configured to do sorption analysis) [44]. Their adsorption studies agreed with those performed by Chen, however, Hill and Seddon found that a rate of 11 water molecules per alumina were adsorbed at low Si/Al ratios. Their results, shown in Figure 18, show that the rate dropped to ~5 water molecules per alumina at higher lower Si/Al ratios, however, they hypothesized that this might be due to extra-framework aluminum atoms being counted in the elemental composition[4].

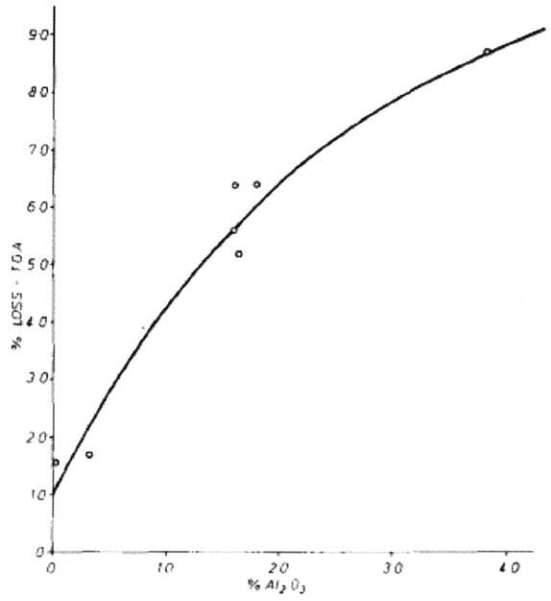

Figure 18. Plot of % weight loss (x-axis) from TGA *versus* % alumina content (y-axis). Adapted from [44].

Hill and Seddon investigated the sorption behavior as well by introducing vapor into the TGA chamber at increasing pressures and showed that as the pressure increased, more water vapor was adsorbed. The data also indicates that water adsorption increases linearly with pressure, which is not seen with nitrogen [21] or with hydrocarbons [44]. This type of adsorptive behavior follows Henry's Law instead of the classical Langmuir adsorption equation [37]. Hill and Seddon hypothesized two possible explanations for this behavior. Their first hypothesis was that the water inside of the pores was actually compressible and, therefore, the density of water in the pores significantly varied with applied pressure. The second hypothesis, which to them seemed

[4] It is generally accepted that extra-framework atoms do not contribute to water adsorption because they do not act as "seed" sights in the way that defect sites do

more probable, may be that the behavior is indicative of surface sorption on nano-sized particles. As the pressure increases, addition layers of water are adsorbed on the surface. This is more evident with nano-sized particles since the surface area to volume ratio is much larger than for micron-sized particles. This effect was also seen with water adsorption on non-porous silica gel materials. An undesirable side effect of their synthesis was that the size of the zeolite particles decreased with increasing aluminum content. Thus, surface sorption would have to increase with increasing aluminum content. Hill and Seddon were unable to show that the adsorption behavior recorded was just surface adsorption and not adsorption into the zeolite pores. Later work performed by Jentys *et al.* argued that water was, in fact, entering MFI zeolite pores instantaneously under ambient conditions [45]. However, Jentys *et al.* were also unable to quantify the amount of water inside of the zeolite pore structure.

Although these studies provide information about the practical usage of zeolites, the sub-nanometer dimensions of zeolites could limit the water transport into the pores. Later experimental results showed that water adsorbs at the hydrophilic silanol defects on the surface and at/around the Al defect atoms on the surface and in the pore network [43, 44].

For our TGA experiments, we investigated the adsorption of water onto non cation-exchanged ZSM-5 zeolites of varying Si/Al ratios before and after a heat treatment. Our goal was to determine the amount of adsorbed water inside of the zeolite pores as well as determining the time scales associated with water entering the inner zeolite pore network. In the experimental results and discussion section in this chapter, we will discuss two different locations where the water is adsorbed (Figure 19).

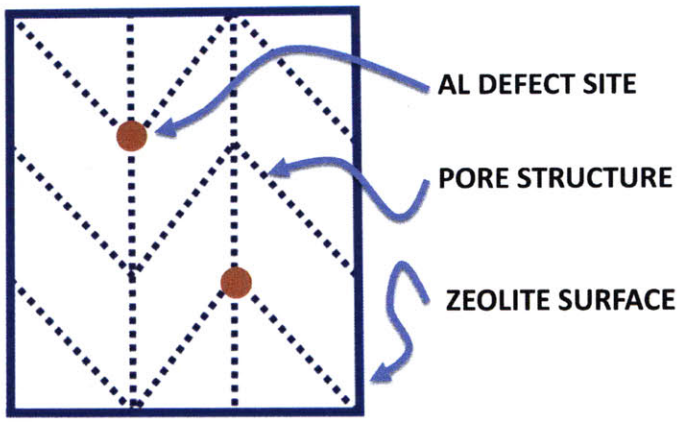

Figure 19. Schematic of zeolite pore structure and the location of the Al defects.

3.2 EXPERIMENTAL PROCEDURE

The thermogravometric analysis (TGA) was performed using a TA Scientific © Q50 Thermogravimetric Analyzer. This general purpose TGA was coupled with a PFEIFFER© Vacuum THERMOSTAR mass spectrometer (MS) to determine which elements and molecules were evaporating from the zeolites during the experiments. The TGA is capable of recording the change in weight with respect to a change in temperature. The software is also capable of determining the derivative of the weight so that specific 'evaporation' events can be identified. This technique is extremely useful for determining the decomposition temperature of polymeric materials [46]. The TGA we used for our experiments is shown in Figure 20.

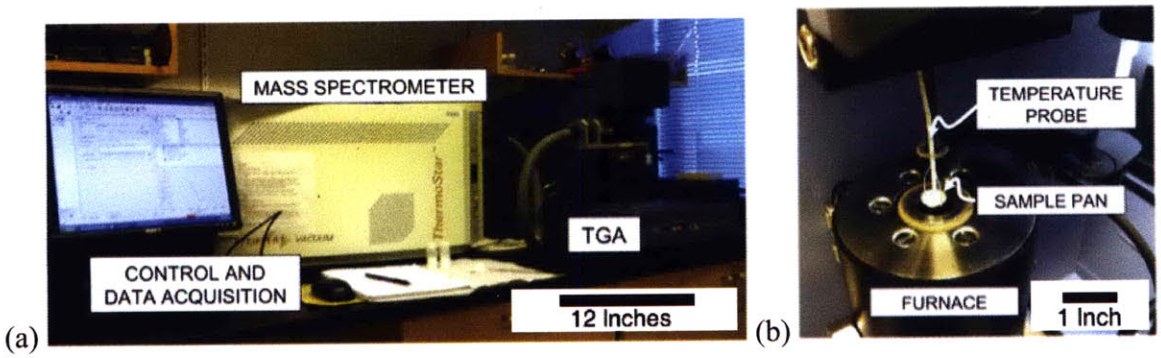

Figure 20. (a) Image of TGA and MS used for experiments (b) Close up view of sample pan being loaded into the furnace.

For our experiments, 10-30 mg of zeolite was loaded into a platinum sample pan (TA Instruments part #952018.906) that was previously used to tare the TGA. We used zeolites commercially obtained from Zeolyst, Inc with Si/Al ratios of 23, 80, and 280 as well as zeolites synthesized in our lab with an Si/Al ratio of ∞. Various TGA experiments were performed with each zeolite, with at least one experiment performed before a heat treatment and then at various times after the heat treatment. The goal of the heat treatment was to expel water, organic material, or other adsorbed elements inside of the zeolite pore so that the transient behavior of water entering and adsorbing into the pores could be investigated. For the heat treatment, we followed the same procedures that are used to calcinate the zeolite pores, which purges the pores of the organic structure-directing agent. The zeolite sample is loaded into a ceramic crucible and

placed into a box furnace that is open to air. The temperature is raised at 1 °C/min to 550 °C and held at that temperature for 6 hours. It is then is slowly cooled to room temperature at 1 °C/min. The entire process takes about 24 hours.

The TGA experiments can run with or without the mass spectrometer (MS). The MS only adds about 15 extra minutes to the experimental procedure so we ran the experiments with the MS. When using the mass spectrometer, helium gas is used to purge the furnace because He gas is lighter than N_2 gas and therefore does not interfere with the MS readings. The mass spectrometer does not provide any quantitative results, *i.e.*, it does not provide any information about the amount of adsorbate leaving the sample. Thus, if two adsorbates (*i.e.*, water and CO_2), are desorbing at the same time (or temperature), the MS cannot differentiate between the different amounts of adsorbates leaving the sample. This ambiguity can create challenges with the experiments when quantitative results are needed. However, if the structure and adsorbing behavior of the sample are known, accurate assumptions can be made (as was the case in our experiments).

The procedure for the experiment is as follows:

- Tare (calibrate) the Pt sample pan in the TGA
- Load 10-30 mg of zeolite that is being investigated
- Load sample into TGA apparatus, wait for weight to equilibrate (~30 minutes)
- Run the experiment (trigger MS to run at start of experiment)
    - Equilibrate at 30 °C
    - Ramp temperature to 850 °C at 10 °C/min
    - Cool to room temperature

Each experiment requires 2 hours. The TGA collects the weight change, the derivative of the weight, and the temperature while the MS collects the ion current associated with water, oxygen gas, and carbon dioxide gas.

3.3 EXPERIMENTAL RESULTS AND DISCUSSION

MFI zeolites with a varying Si/Al ratio were investigated. MFI 23 (Si/Al -23, Zeolyst, Inc) is the least hydrophobic MFI zeolite of our samples so it was expected to have the highest

adsorbed water content. In Figure 21, the derivative weight loss as a function of temperature for MFI 23 is shown.

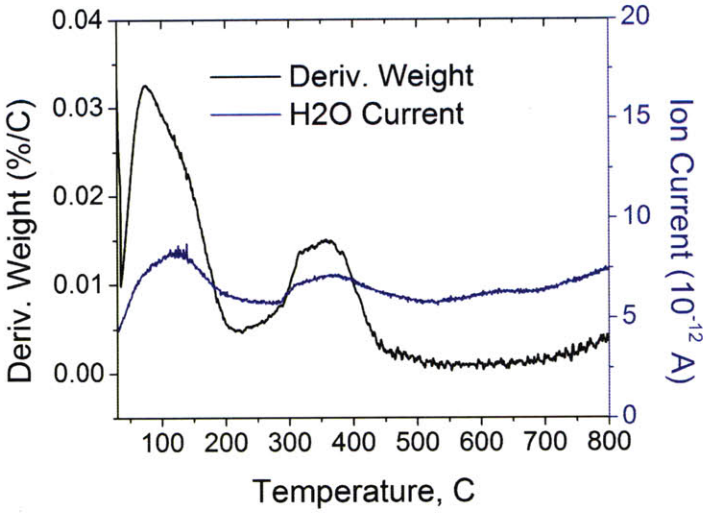

Figure 21. Derivative weight loss as a function of temperature for MFI 23 before heat treatment. The ion current associated with water is shown in blue.

The data indicates that there are two events during which significant weight loss occurs, with the first occurring from ~30 °C to ~180 °C and the second occurring between ~275 °C to ~450 °C. When the TGA analysis is coupled with the MS (Figure 21b), it can be seen that both peaks are associated with increases in the ion current of water. Therefore, we hypothesized that the majority of the weight change is due to water leaving the zeolites. The two evaporation events suggest that water is adsorbed in two different locations: on the surface and confined in the zeolite pore network. The first peak is associated with adsorbed water that is evaporating from the surface. As the water can be confined to the Al defects within 5.6 Å pore structure, it does not seem improbable that more energy would be required for the water to exit the pore system, resulting in the high-temperature second evaporation event. To investigate the time-dependent behavior of adsorption, we heat-treated the zeolite (as described on page 37) and reran the TGA experiment. The results, Figure 22, show only the first evaporation event occurring.

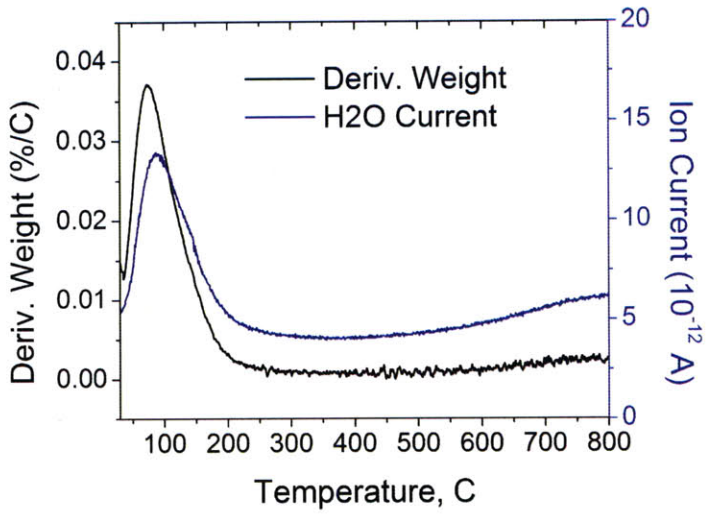

Figure 22. Derivative weight loss as a function of temperature for MFI 23 <u>after</u> heat treatment.

When the TGA experiment is coupled with the MS, it clearly shows that only the evaporation peak obtained is associated with water desorbing from the outer surface of the zeolites. The TGA experiments were repeated at time intervals of 36 and 84 hours after the heat treatment, however, the secondary peak does not appear. We believe this result indicates a diffusion limitation that was restricting the water from freely moving into the zeolite pores.

Based on the available experiments and simulations investigating the diffusion of water in MIF zeolite pores, the diffusivity values are on the order of ~10^9 m^2/s. A summary of the data is shown in Table 6.

Table 6. Diffusivities of water inside of MFI zeolite pores using various techniques [47-50]

Zeolite	Diffusivity (10^{-9} m^2/s)	Technique	Authors
MFI (Si/Al - ∞)	1.94	MD	Ari *et al.* 2009
MFI (Si/Al - ∞)	8.83	GCMC	Fleys *et al.* 2004
MFI (Si/Al - ∞)	1.7	Expt (PFG-NMR)	Bussai *et al.* 2002
MFI (Si/Ai - ∞)	8.6	MD	Demontis *et al.* 2003
MFI (Si/Al – 191)	0.78	MD	Ari *et al.* 2009
MFI (Si/Al - 95)	0.35	MD	Ari *et al.* 2009

Using the diffusivities found and applying Einstein's relation under the assumption that Fickian diffusion conditions hold [48], characteristic time scales for the diffusion of water in these types of zeolites were determined. With the size of zeolite being between 1 - 10 μm, this time scale should be between 1-100 μs. With the times we investigated (12 hours and greater), this should imply that water has completely diffused through the porous structure of the zeolite. However, the TGA experiments contradict this. Thus, our interpretation of the experimental data from the TGA and the diffusivity values found in literature is that an energy barrier exists which is restricting water from entering into the zeolite pores.

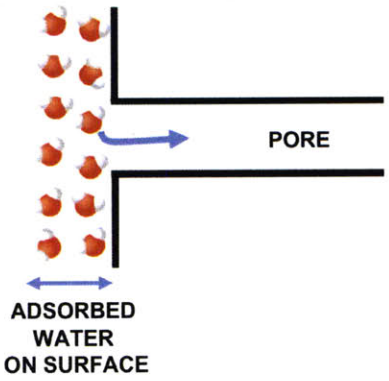

Figure 23. Schematic of possible state of adsorbed water on surface of the zeolite after the heat treatment.

It is clear that the water still adsorbs to the surface of the zeolite crystal. Although MFI zeolites are considered hydrophobic, the surface of every zeolite is hydrophilic due to the high

density of silanol defects [44]. These defects occur because as the synthesis stops, Si-O groups are left unpaired. Therefore, the groups have an increased affinity for cations and the groups usually accept a free proton (H^+) from the solution. The O-H terminated groups provide a site for water molecules to adsorb to and, thus, the surface becomes hydrophilic. These groups rarely occur inside of the pore structure. This surface adsorption behavior is shown in the schematic in Figure 23. The surface adsorbed water molecules create a concentration gradient, which should force water to diffuse into the zeolite pores (where water is absent). As explained earlier, this does not immediately occur. We speculate that the hydrogen-bonding network of the water adsorbed onto the surface creates the energy barrier prohibiting the water molecules from freely diffusing into the pores. There has been experiments and simulations that show this effect for completely hydrophobic MFI zeolites [51, 52], however, not for lesser hydrophobic MFI zeolites. Although some critical Si/Al ratio should exist for when it is more energetically favorable for the water to enter the pore (*i.e.,* the defect density of the Al sites is much larger), we speculate that it is be below the Si/Al ratios that were currently investigated.

As the Si/Al ratio increases, the zeolite becomes more hydrophobic [21]. Therefore, less water should be adsorbed not only on the surface but also inside of the pore structure. We chose MFI 80 (Si/Al – 80) zeolites commercially obtained from Zeolyst, Inc to study next. In Figure 24, the results from the TGA experiments for MFI 80 before the heat treatment are shown along with the MFI 23 sample for comparison.

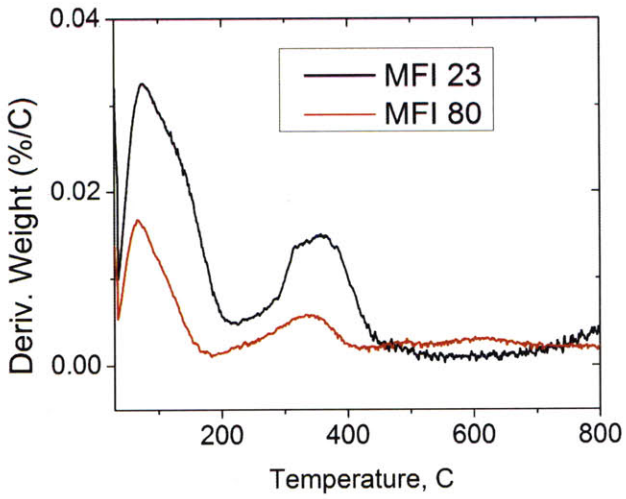

Figure 24. Derivative weight *versus* temperature for MFI 80 (in red) and MFI 23 (in black) before heat-treatment. Note the decrease in peak magnitude meaning less overall water adsorption.

The two evaporation peaks are observed as we increase the Si/Al ratio, however, the overall magnitude of the peaks decreased. This result suggests an expected decrease in water adsorption both on the surface and in the pore structure. After heat-treating the MFI 80 zeolites, the secondary evaporation peak disappears (shown in Figure 25). Although this was expected from the behavior observed with the MFI 23 zeolites, this data reinforces the idea that the hydrogen-bonding network of the adsorbed water prohibits the water from freely diffusing into the zeolite pores.

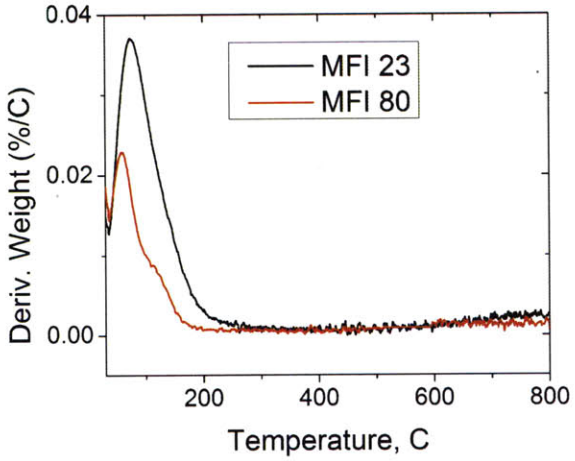

Figure 25. Derivative weight *versus* temperature for MFI 80 (in red) and MFI 23 (in black) after heat treatment.

If the aluminum is not added during the synthesis process, the zeolite pore structure becomes completely hydrophobic [53]. With an infinite Si/Al ratio, a significant pressure (>40 MPa) is required to force water into the pores [21]. Therefore, it is expected that water will only be adsorbed on the surface of these types of MFI zeolites. In Figure 26, the derivative weight as a function of the temperature for MFI ∞ (Si/Al - ∞) zeolites before heat treatment (Figure 26a) and after heat treatment (Figure 26b) is shown. Only one evaporation peak is present for both before and after the heat treatment, which suggests that water is only adsorbed on the surface of the zeolites. This analysis provides more evidence that the secondary peak of the MFI 23 and MFI 80 zeolites is caused by water adsorbed inside of the zeolite.

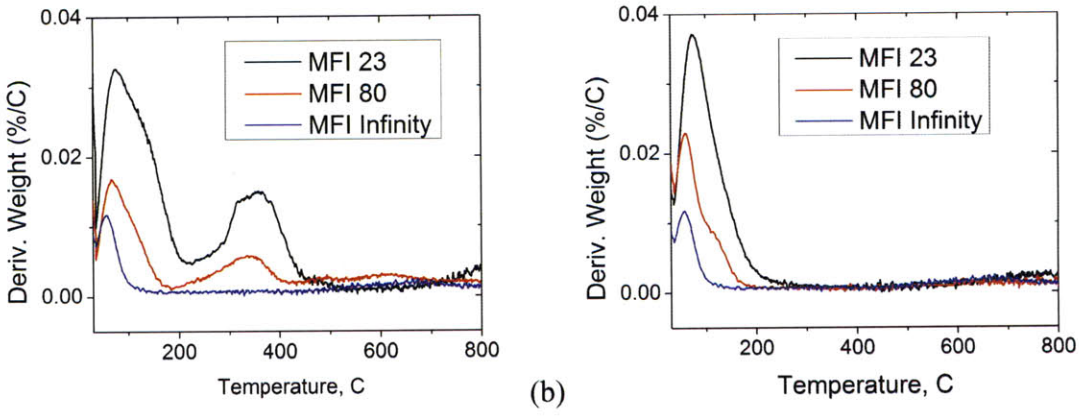

Figure 26. (a) Derivative weight *versus* temperature for MFI ∞ (in blue) before heat treatment (b) Derivative weight *versus* temperature for MFI ∞ (in blue) after heat treatment.

The amount of water in the zeolite pores can be estimated from the TGA experiments. However, first, an assumption of the density of water inside of the pores must be made. Due to the confined nature of the water molecules, assuming that the density of water remains the same as bulk would be incorrect. Therefore, as a first estimate, we assume that the water molecules in the zeolite pores create a single file chain. This type of behavior has been seen with MD simulations of zeolite pores [52] and carbon nanotubes [54]. Applying this assumption, we estimated that the density of water inside of these MFI zeolite pores is 0.433 g/cm^3. Next, the amount of water that desorbed (or evaporated) during the secondary peak in the TGA data[5] was calculated. The changes in weight can be seen if the normalized weight loss (current weight/initial weight) is plotted as a function of the temperature, which is shown for all three zeolites in Figure 27.

[5] We calculated the weight change by finding the temperature range that this secondary peak occurred. For the MFI 23 zeolites, this occurred between 220 °C and 445 °C. For the MFI 80 zeolites, this occurred between 190 °C and 410 °C.

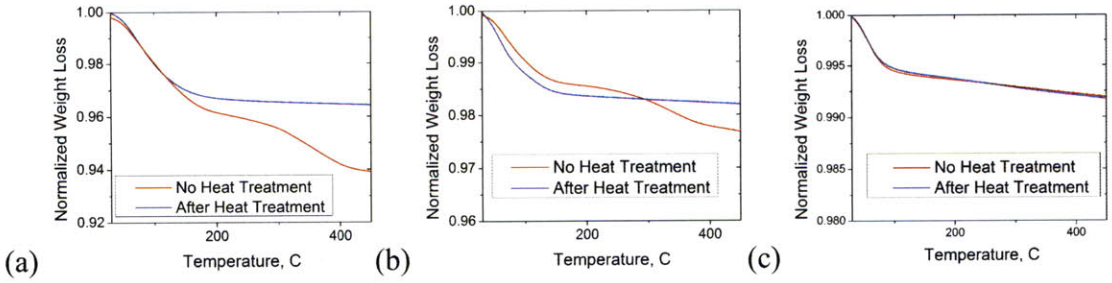

Figure 27. Normalized weight loss *versus* temperature for (a) MFI 23 (b) MFI 80 and(c) MFI ∞. Note that there is no difference before and after the heat treatment for MFI ∞, implying that water is never adsorbed in the pores.

After we determined the weight loss for the secondary peak, we estimated the volume of the pores that was filled prior to the heat treatment. As expected, the percent pore volume filled in the zeolites increased as the hydrophobicity decreased. The compiled results are shown in Table 7.

Table 7. Approximate percentage of zeolite pore volume filled for varying Si/Al ratios prior to heat treatment.

	Total Adsorbed Water, %	Water in Zeolite Pores, %	Pore Volume Filled, %
MFI 23	6.1	2.3	70.8
MFI 80	2.2	0.9	25.4
MFI ∞	1.3	0.0	0.0

3.4 SUMMARY

In this chapter, the effect of the Si/Al ratio on the adsorption of water on the surface and in the pores of MFI zeolites was investigated. Although it is well known that the Si/Al ratio affects the hydrophobicity of zeolites, it was unknown if water was adsorbed inside of the pore structure. We did thermogravimetric analysis of zeolite samples that were in ambient conditions for time periods of 12 hours to 6 months. For the less hydrophobic zeolites (≤ 80), a secondary

evaporation peak was observed if the zeolite was left in open air for 6 months. The secondary peak was not observed for the completely hydrophobic zeolite. However, if the zeolites were tested within 84 hours after the heat treatment, the secondary peak was not observed. This data suggests that the secondary peak is associated with water adsorbed inside of the pores. An energy barrier also seems to exist that prevents the water from freely diffusing back into the pores and we speculate that it arises from the hydrogen bonding network of the adsorbed water on the surface of the zeolite crystals. Finally, we estimated the amount of pore volume that is filled with water for the zeolites that were left in ambient conditions for at least six months. As the Si/Al decreases, the amount of pore volume filled increases. For the least hydrophobic MFI zeolite (Si/Al – 23), the pore volume filled was estimated to be ~70% while for the MFI 80 sample, the pore volume filled was estimated to be ~25%.

Chapter 4

4. Pressure Infiltration Studies

4.1 PAST RESEARCH

The investigation of pressurized water transport into zeolite pores is a complex and ongoing research topic. In 2001, Eroshenko *et al.* were the first to investigate this topic using hydrophobic zeolites for the application as an energy recovery device [55]. They used small amounts (<0.2 g) of hydrophobic MFI zeolites as well as hydrophilic zeolite-β and Na-ZSM-5 zeolites that were encapsulated in a polypropylene (PP) cell with 1 mL of deionized water. They applied pressure and monitored the change in volume of the PP cell by using a modified mercury porosimeter. From these tests, they were able to determine the infiltration pressure, that is, the pressure that is required to force water into the pores. Their compression-volume curves are shown in Figure 28.

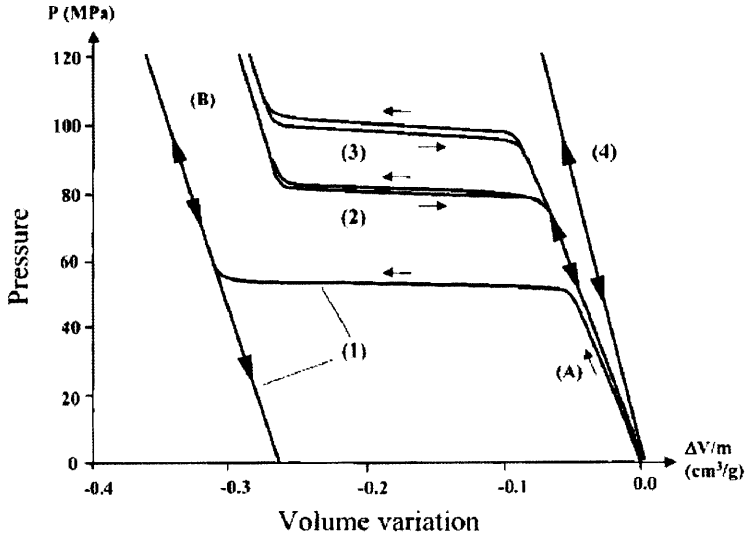

Figure 28. Pressure-volume isotherm of the various "water-hydrophobic zeolite" systems. (1) zeolite-β (2) MFI (OH^- based) (3) MFI (F^- based) (4) Na-ZSM-5. Note that for (1), (A) symbolizes the step before intrusion and (B) the step after intrusion [55].

The two hydrophilic zeolites (zeolite-β and Na-ZSM-5) exhibited two different infiltration behaviors. The Na-ZSM-5 (Si/Al – 27) behavior has the same compressibility as a pure water

sample, which implies that the pore volume was completely filled with water prior to an applied pressure. The zeolite-β sample, however, initially exhibits a hydrophobic behavior. During the first compression cycle, approximately 50 MPa are required to force water into the pores. However, once the water enters the pores, it stays adsorbed inside of the pore structure and subsequently exhibits infiltration behavior that is the same as Na-ZSM-5. This type of behavior is usually described as a 'molecular bumper', meaning that the zeolite absorbs water (and therefore energy) in a one-time event in the same way a car bumper adsorbs energy in a crash. The hydrophobic MFI zeolites exhibit behavior of which is described as a 'molecular spring'. A significant amount of applied pressure (> 80 MPa) is required to infiltrate the pores. However, as the pressure is relaxed, the water exits the pores. The behavior is completely repeatable. Since the MFI (F^- based) zeolite exhibited the largest infiltration pressure and was therefore the most hydrophobic, Eroshenko *et al.* assumed that the contact angle at the solid-liquid interface would be 180°. Thus, from the classical Laplace-Washburn equation, they found that the surface tension value was 13.9 mN/m. This value is approximately 5 times less than the accepted bulk value for surface tension. Although the authors used continuum relations which may not be accurate at this scale, they did expect the value of surface tension to decrease. They explain that surface tension should be proportional to the number of OH^- bonds that have to be broken around each water molecule and thus is dependent on the coordination number. For water molecules inside of the pores, the coordination number should decrease due to the confinement.

There has been a variety of experimental [56-59] and simulation [60-62] work performed in this field over the last decade. However, of these, the combined experimental and simulation paper by Qiao *et al.* is most similar to the work we subsequently performed [63]. Qiao *et al.* used MFI zeolites with a Si/Al ratio of 280 obtained from Zeolyst, Inc for their infiltration experiments. Since the behavior was hydrophobic (defined previously by Eroshenko *et al.*), this was a model zeolite to study the repeated infiltration characteristics. Their setup was a basic stainless steel pressure vessel, shown in Figure 29, that enclosed a water/zeolite mixture. Pressure was applied and the displacement was measured with an Instron testing apparatus. They performed infiltration experiments at various displacement rates to determine the changes in behavior.

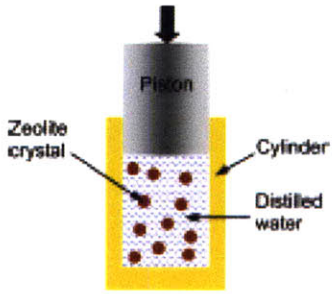

Figure 29. Schematic of experimental setup used by Qiao *et al* [63].

Prior to the experiments, the zeolites were dried in a vacuum at 150 °C and then flushed with a silicon tetrachloride vapor at 400 °C for an hour. This was done to remove all organic material as well as any water from inside of the pores. The zeolites (approximately 0.5 g) were mixed with deionized water and the experiments were conducted using displacement rates varying from 0.03 mm/min to 30 mm/min. The specific infiltration curves (normalized by the weight of the zeolite for each experiment) are shown in Figure 30 and closely resemble an IUPAC type IV adsorption isotherm.

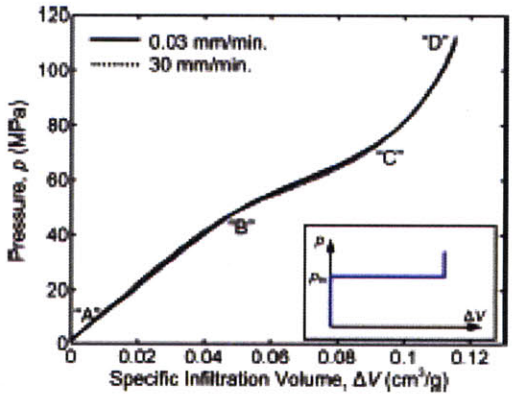

Figure 30. Water sorption isotherms for the MFI 280 zeolites. The inset depicts what should occur if continuum approximations are applied [63].

Figure 30 shows that the infiltration characteristics do not follow what is predicted by the Young-Laplace equation (Figure 30 inset). Instead, it seems that there is a dependence of length on the infiltration isotherm. There is also a lack of rate dependence on the infiltration isotherm. Again, this deviates from what is expected from continuum hydrodynamics. According to Hagan-Poiseuille flow, an increase in the volumetric flow rate causes an increase in the pressure

drop and therefore should cause a change in infiltration behavior. However, even though the infiltration rate of the two isotherms varies two orders of magnitude, the isotherms do not change significantly. Qiao *et al.* then performed MD simulations on an 8.3 Å diameter pore inside of silicon dioxide (this was deemed "as a close analog to the MFI zeolite nanopore"). Initially, water was not present in the pores. To increase the pressure, the volume of the reservoir was decreased and the pressure was calculated from the state function of water. As the pressure in the 'chamber' increased, the potential energy of the water molecules also increases until the water molecules have enough potential energy to overcome the barrier that is preventing them from entering the pores[6]. They speculate that the energy barrier arises from two sources. First, as the water molecules must break from their bulk structure to fit in the confined zeolite pores. Thus, some hydrogen bonds must be broken. The second source originates from van der Waals and electrostatic interactions that the water is subjected to inside of the pore. These two effects combined provide an effective solid-liquid interfacial energy ($\Delta\gamma$). Indeed, after the analysis, they found that the $\Delta\gamma$ term is positive, meaning that an energy barrier exists and the pore is hydrophobic. From this analysis, the infiltration pressure should only be ~1.11 MPa. The MD results show that water does begin to infiltrate into the pores at this low pressure (Figure 31b).

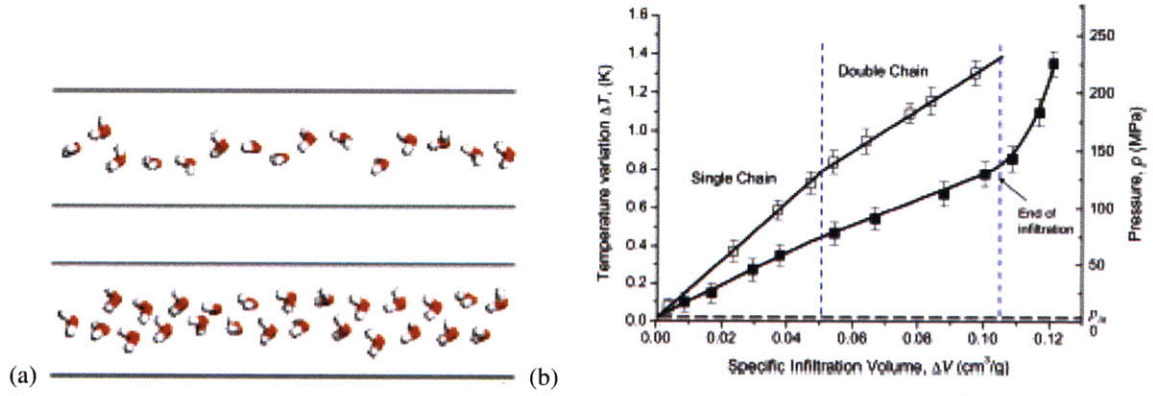

Figure 31. (a) The formation of a single chain of water molecules in pore at ~50 MPa (top) and a double chain of water molecules at ~125 MPa (b) MD results of the pressure (solid symbol) and temperature (open symbol) as a function of the specific infiltration volume [63].

The infiltration behavior into the pore behaved in a 'dislocation-like' propagation. The water chain jumped in a step-like fashion to accommodate for the new water molecules entering the

[6] We suspect that a similar type energy barrier is prohibiting the water from diffusing into the less hydrophobic zeolite as well.

pore. Once the single chain spanned the length of the pore, a secondary infiltration event occurs as a second chain of water molecules begins to fill the pore. After this secondary infiltration event, the pore cannot accommodate any more water molecules and therefore the infiltration ends. Although the MD simulation does not exhibit the exact same infiltration behavior witnessed in experiments, it is very similar. Figure 31b also shows that the pressure increases nearly linearly as a function of the specific infiltration volume. This implies that not only does the infiltrated chain need to overcome the infiltration pressure but also some barrier that varies with the volume. This can be deduced as a sort of column resistance, arising from the interactions of the chain with the interior surface of the pore. Qiao *et al.* quantified this column resistance and then altered the classical Young-Laplace equation as follows:

$$p = \frac{4(\Delta\gamma + \eta L)}{D} \tag{2}$$

where η is denoted as the column resistance term, L is the length of the pore, p is the pressure, D is the diameter of the pore and $\Delta\gamma$ is the surface-liquid interfacial energy term. This shows that a new mechanism controls the propagation of water at this length scale.

In this chapter, we focus on determining the amount of water in the MFI zeolite pores and how the Si/Al ratio affects this amount. Also, since it is also unknown as to how the Si/Al ratio (specifically, the Al defect sites) affects the transport of water molecules inside the pores, we investigate the shape and characteristics of the infiltration isotherm for various Si/Al ratio zeolites.

4.2 EXPERIMENTAL SETUP

We fabricated a custom-designed pressure vessel that was capable of holding an internal pressure of 200 MPa and allow for simple sample loading and removal. The concept of the pressure vessel is shown in Figure 32.

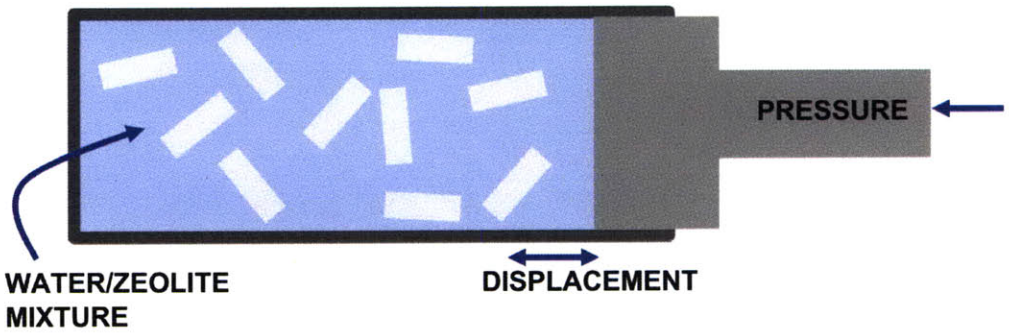

Figure 32. General schematic of pressure vessel for infiltration experiments.

We machined the pressure vessel from 304 stainless steel which was chosen for its high strength, corrosion resistance and machinability. The inner diameter of the pressure was made to be 0.502" and polished with burnishing tools. The pistons were also made from 304 stainless and had grooves machined into them to hold two glass-filled PTFE backup rings and a urethane (90 Shore A hardness) o-ring. The other dimension of the o-ring was 0.504" so it had to compress slightly to fit into the pressure vessel. This level of precision was required so that the vessel would not leak under high (> 100 MPa) pressure. Polymer o-rings usually are not used for this type of setup, however, we did not observe any leaking during the experiments. O-rings and backup rings were replaced after every experiment to decrease the chance of o-ring failure.

The pressure vessel needed to be interfaced with an apparatus to apply a force and monitor displacement. For our experiments, we used an Instron 5582 running the BlueHill 2 software. The Instron is capable of applying loads of 100 kN (although we only needed 20 kN). We used the Instron to measure displacements with a resolution up to 0.01 mm. To determine the infiltration behavior into the pores, we used the 'compliance correct' feature on the software. The compliance we corrected for was a control sample of 10 mL of water. Since every experiment used 10 mL of water, we used to software to remove this displacement from the experiments. Therefore, any additional displacement (due to water infiltrating into the zeolite pores) would be recorded as the only displacement in the data. This removes time-consuming post processing of the raw data and largely removes a source for any error in the data.

For the experiments, we used 1.0 g to 2.5 g of zeolites immersed in class 2 deionized water (VWR). Prior to the experiments, the zeolites were heat-treated according to the procedure (described is section 3.2). A specific mass of zeolite was weighed and poured into a glass beaker

containing 10 mL of the deionized water. The solution was mixed for ~30 minutes with a magnetic stir rod at 200 RPM to create a well-dispersed mixture. The solution was then transferred to the pressure vessel. Great care was taken so that macro scale air bubbles (and air in general) were not introduced into the vessel. The vessel is then sealed with a second piston and aligned so that the solution is approximately in the center of the vessel. The vessel is then placed into a holder to maintain an upright position and transferred to the Instron 5582. A schematic of the actual vessel used as well as a picture of the experimental setup is shown in Figure 33.

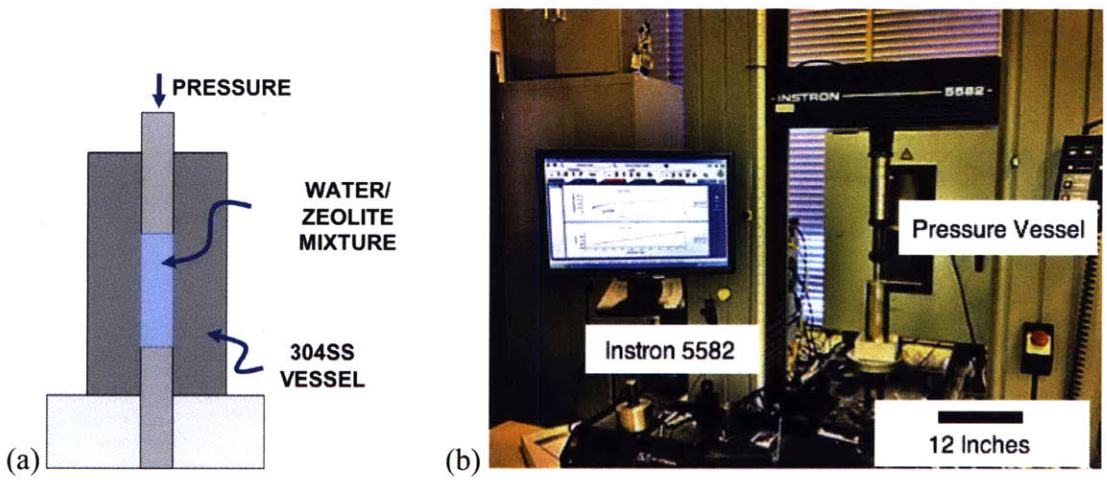

Figure 33.(a) Schematic of the two-piston pressure vessel used for infiltration experiments (b) Picture of the Instron 5582 with pressure vessel loaded into the apparatus.

The zeolites that were used in this initial study were all commercially obtained from Zeolyst, Inc. The Si/Al ratios of the MFI zeolites were 23, 80 and 280.

4.3 EXPERIMENTAL RESULTS AND DISCUSSIONS

We first investigated the role of displacement rate on the infiltration isotherms. We varied the displacement rate from 1 mm/min to 30 mm/min and the data is presented as a volumetric infiltration rate. The infiltration rate into the pores is dependent on the displacement rate and the cross-sectional area of the pressure vessel. Therefore, the volumetric infiltration rate is a better metric to use for comparison with other experiments. The zeolite used for this experiment was the MFI 280 (Si/Al – 280) and the amount was varied between approximately 1 g and 2.5 g. The data is plotted as pressure as a function of the specific infiltration volume (SIV). The SIV is a

volume that is normalized by the amount of zeolite used for each individual experiment. Figure 34 shows the infiltration isotherms for varying infiltration rates.

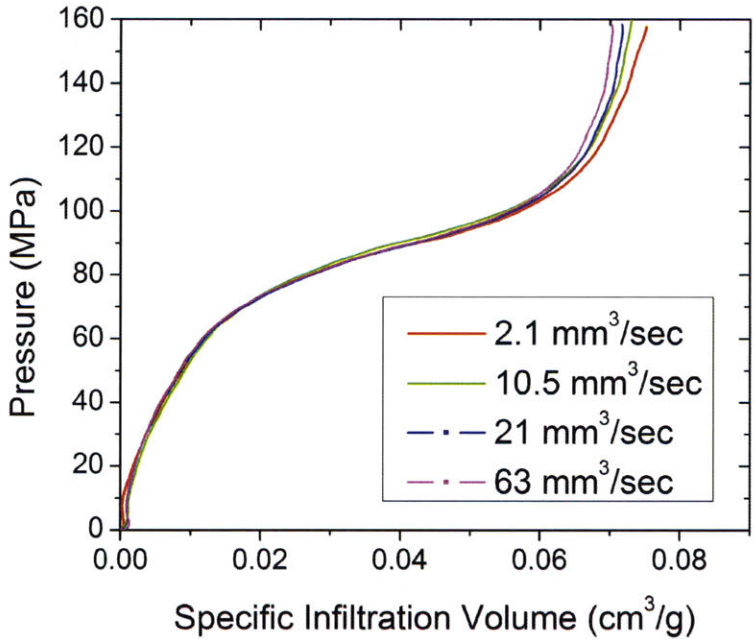

Figure 34. The water infiltration isotherms for MFI 280 for varying infiltration rates.

Similar to the work by Qiao *et al.* [52], no obvious change in the infiltration isotherms was observed as the infiltration rate is changed. There are some repeatable differences in the final infiltration volume, however, it is unclear whether these volumetric differences are artifacts of the Instron data collection or if it is a real phenomenon. As stated previously, this behavior does not follow continuum hydrodynamics. Also, the final infiltration volume is lower than what groups have previously reported. We believe that the values we obtained for the infiltration volume at 160 MPa (0.072 cm^3/g) are correct[7]. Although we plan on investigating the reason that the infiltration isotherms do not change a function of displacement rate, we were able to determine that we only need to use one rate to accurately characterize the infiltration isotherms. Therefore, in all subsequent experiments, we only used a volumetric displacement rate of

[7] A possible explanation as to why the value is lower might be because we didn't perform the same cleaning techniques as other authors. However, from the TGA experiments, it seems that most of the water is absent from the pores after the heat treatment so we are confident the full pore volume is accessible.

2.1 mm^3/sec (this corresponds to a 1 mm/min displacement rate). The shape of the infiltration isotherm is similar to the work by Qiao *et al.* [52].

For our initial experiments, we studied the infiltration behavior of two other MFI zeolites that were less hydrophobic, MFI 80 (Si/Al – 80) and MFI 23 (Si/Al – 23). Although hydrophobic MFI zeolites have been studied in detail [51, 53], less hydrophobic zeolites aren't ideal as energy recovery devices since they seem to adsorb water almost instantaneously and therefore haven't been extensively studied. On the other hand, this type of behavior can be ideal for a water desalination membrane since no additional pressure is required to fill the zeolite with water. However, it is unknown whether the full available pore volume is instantaneously filled with water prior to an application of pressure or at which Si/Al ratio the zeolite changes from hydrophobic infiltration to a 'hydrophilic-like' infiltration[8].

The infiltration isotherms of MFI 23, MFI 80 and MFI 280 are shown in Figure 35. The difference in infiltration behavior is significant. The less hydrophobic zeolites do not exhibit the characteristic type IV adsorption isotherm that the hydrophobic zeolites exhibit. In fact, the behavior is not characteristic of any known adsorption behavior.

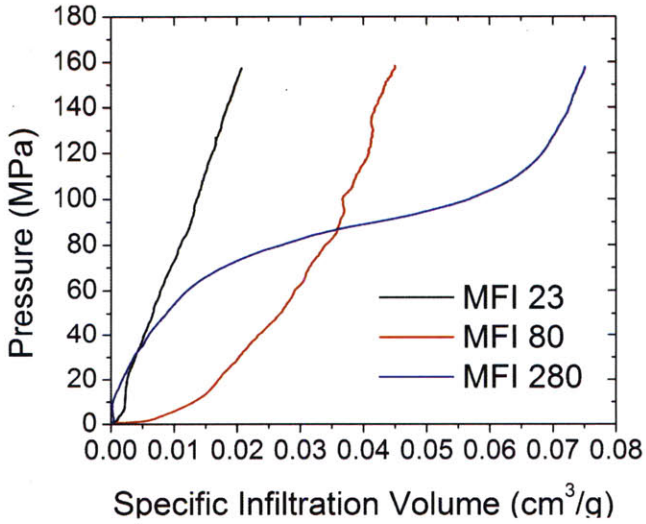

Figure 35. Specific infiltration volume as a function of pressure for various MFI zeolites.

[8] The terms hydrophobic and hydrophilic are not proper to use in describing this behavior, however, the adsorption community has accepted them. A more proper way to describe the difference between the infiltration behaviors of these zeolites is hydrophobic and less hydrophobic.

The MFI 23 sample shows the smallest increase in specific infiltration volume as the pressure increased. Previous experiments with this low Si/Al ratio have shown that the pore volume is completely filled instantaneously before a pressure is applied. Since we removed the volumetric displacement due to the compression of water, we speculate that there are two possible explanations for this behavior. First, there are completely hydrophobic areas of the pore volume where the Al defects are a significant distance apart so the water molecules adsorbed to each site cannot interact and form a bridge [37, 47]. Therefore, this infiltration behavior could be described by the filling of these areas. Secondly, as seen in the work but Qiao *et al.* [52], the infiltration could be characterized as the infiltration of two chains. Therefore, this behavior could be described by the total filling of the pore volume by the secondary chain of water molecules. We plan on investigating this further by using molecular dynamic simulations to model this infiltration behavior. As the behavior is repeatable, we believe that the zeolite pore network does not stay completely filled, even after the infiltration experiments. The MFI 80 sample exhibits behavior that is similar to MFI 23 but with an increased infiltration volume. At lower pressures (<20 MPa), nearly 50% of the available pore volume[9] is filled. Above 20 MPa, the infiltration behavior is very similar to the MFI 23 sample in that the small amount of hydrophobic pore volume within the pore structure is being filled with water. This infiltration was repeatable so, again, we believe that the pore network does not stay completely filled without an applied pressure.

From these results, we are able to estimate the amount of pore volume that is filled prior to the experiments. We assume that the MFI 280 zeolite is completely hydrophobic [63] and thus the specific infiltration volume at 160 MPa is the total available pore volume for the water to fill (denoted at V_a). Then, by estimating the specific infiltration volume of the MFI 23 and MFI 80 samples at 160 MPa (denoted at V'), we can determine the pore volume that was filled during the experiment. Therefore, the pore volume that is filled prior to the experiment (denoted as V_f) is:

$$V_f = \frac{V_a - V'}{V_a} \tag{3}$$

[9] Available pore volume in this context means pore volume that is not filled with water prior to the experiment

Table 8 shows the estimated values for these volumes as well as a comparison to the TGA experiments performed in the previous Chapter 3. The estimated volume filled prior to the infiltration experiments and TGA experiments are in close agreement. Therefore, we have two independent experiments that can be used to determine the amount of water that is filled inside the pores in an ambient atmosphere during a long period of time.

Table 8. Compiled values of estimated pore volume filled with water for TGA and PI experiments.

	% Pore Volume Filled PI	% Pore Volume Filled TGA
MFI 23	72.2	70.9
MFI 80	34.3	25.4

4.4 SUMMARY

In this chapter, the effect of Si/Al ratio on the amount of water that filled the MFI zeolite pores prior to an applied pressure was investigated. We built a custom pressure vessel that was used to hold a water/zeolite mixture to pressures of 160 MPa. Using an Instron 5582 testing apparatus, we were able to determine the infiltration isotherm for MFI 280, MFI 80 and MFI 23 zeolites. The measured infiltration isotherms were repeatable for a variety of zeolite masses. Assuming that water is not inside of the MFI 280 pores, we could estimate the pore volume that was filled for the less hydrophobic zeolites. The least hydrophobic MFI zeolite (MFI 23) had approximately 73% of the pore volume filled prior to an applied pressure and the MFI 80 zeolite had approximately 34% of the pore volume filled prior to an applied pressure. These values match well with the values we estimated from the TGA experiments described in chapter 4. We are planning to perform MD simulations on the infiltration of water into MFI zeolite pores.

Chapter 5

5. Defect-free Membrane Fabrication

The overall goal of the previous chapters was to understand the adsorption and transport mechanisms in zeolite pores. Next, we will apply that knowledge to increase the permeability of reverse osmosis membranes. Even though the zeolite structure should allow for increased permeability and salt rejection, previous experimental research has shown that fabricating RO membranes that exhibit these characteristics is not trivial. We propose a novel method of creating thin, oriented zeolite membranes that limit the transport of the water through the zeolite pores. This method avoids secondary growth techniques that create nanometer-sized intercrystalline defects. The idea of this method is to interface it as the active desalination layer in a gradient ceramic membrane that is currently being developed at the King Fahd University of Petroleum and Minerals.

5.1 FABRICATION BACKGROUND AND DETAILS

The schematic of the proposed membrane is shown in Figure 36. The idea of the membrane is to orient a monolayer of zeolites that is less than 200 nm in thickness. A polymer that is impermeable to water and salt ions must be deposited between the zeolites. Since permeability is directly dependent on the thickness of the membrane, the thickness must be minimized. We chose to achieve membranes with a thickness of 200 nm which corresponds to the average thickness of reverse osmosis membranes [8].

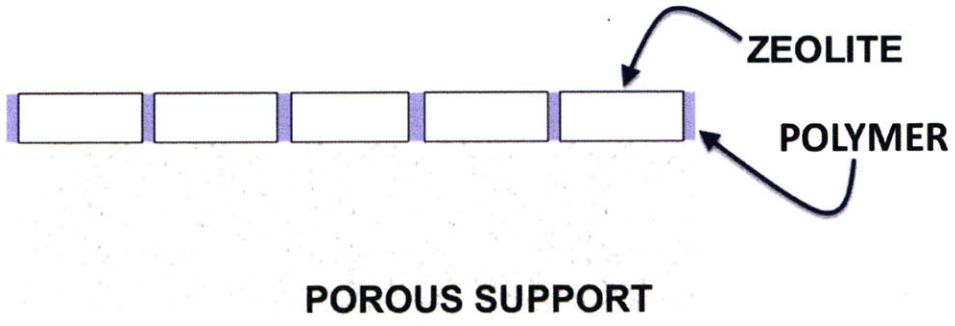

Figure 36. Schematic of ideal membrane for RO. The polymer must be water and salt impermeable.

There are different ways to achieve an oriented layer of zeolites onto a surface. The most widely used method is by functionalizing and seeding of the support [64]. Figure 37 shows SEMs of typical coverage and orientation of this technique.

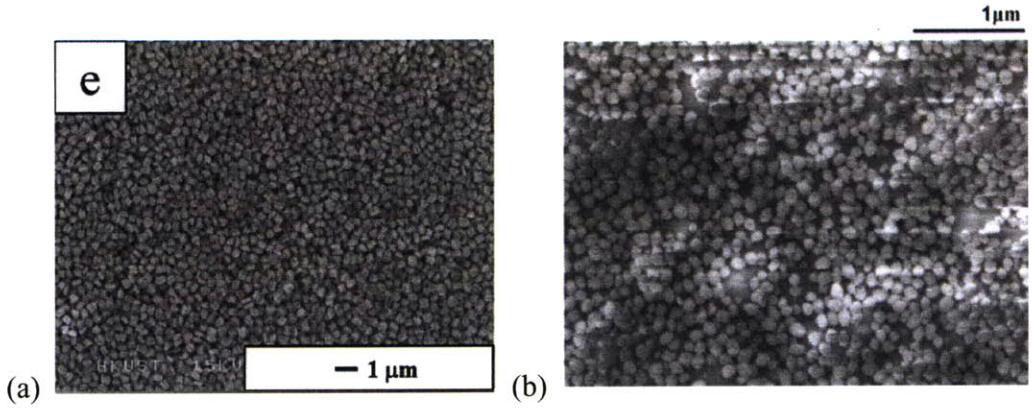

Figure 37 (a) Oriented layer of MFI zeolites on a silicon support using mercapto-3 as a binding agent [64] (b) a-oriented MFI zeolites on a silicon support using 3-chloropropyltrimethoxysilane as a binding agent [65]

The high magnitude of coverage and level of orientation of these types of membranes is not consistently achievable for surface areas greater than 1 cm^2. In addition to this, in order to create a membrane from these seed layers, a secondary hydrothermal synthesis must be performed (also known as a secondary growth) to fill the intercrystal gaps. However, as described in the Chapter 1, this creates nanometer-sized defects which decreases the intrinsic selectivity of the zeolite pores. The process of functionalizing the surface also requires inert atmospheres and, therefore requires controlled environments (such as a glove box). Groups later attempted to control synthesis conditions so that oriented zeolite layers would grow directly from zeolite supports[10] [29, 53, 66]. These membranes tend to perform well for gas separation membranes, however, the membranes had limited performance for RO due to their increased thickness [67].

A novel technique for orienting a thin layer of zeolites was introduced by K.B. Yoon's group in 2007 [68]. The technique involves depositing zeolites onto a surface and rubbing the surface with either a gloved finger or some type of rubber pad (this method is aptly known in the

[10] Although most groups would still lay down a layer of zeolites as a seed, this did not enhance the orientation. Instead, it limited the thickness and defect density of the membranes because the process averted the nucleation portion of the synthesis.

research community as the "rubbing method"). The method, as archaic as it sounds, produces high quality of oriented monolayers of zeolites on various substrates [69]. A progression of the technique is shown in Figure 38. First the surface (in this case a silicon wafer) must be appropriately cleaned of any organic material (for more details on this cleaning process, see appendix 1). The synthesized zeolite powder is then deposited onto the surface manually and finally the zeolite powder is crushed and rubbed over the surface.

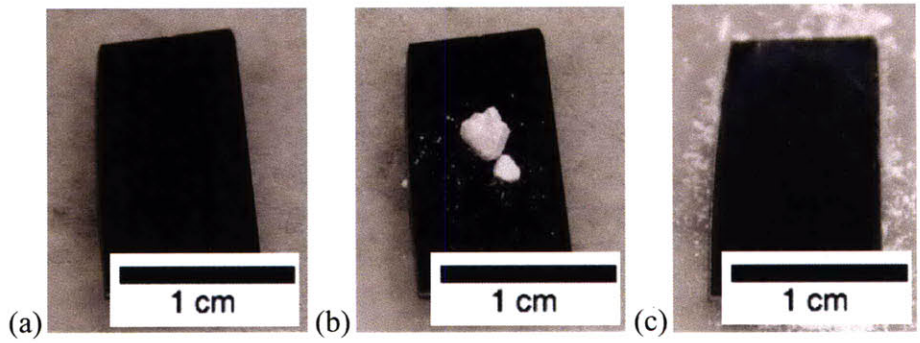

Figure 38. (a) Picture of a cleaned silicon wafer section (b) Zeolite powder deposited onto the surface of the cleaned silicon wafer (c) The final oriented zeolite layer on the silicon surface.

The surface is rubbed until the color of the wafer becomes a 'milky' white. The adhesion between the zeolite and the surface can be enhanced if the zeolite does not adhere correctly[11]. An adhesion polymer (such as polyetherimine or polyvinylalchol) can be spin coated onto the substrate. This methodology is described further in Appendix 1.

A caveat of this type of orientation is that the zeolites need to have a small size distribution. This is not emphasized in literature, however, it is one of the most important requirements in creating an oriented layer of zeolites. Even an average size deviation of ±100 nm will yield less than satisfactory results. Also, in order to obtain a specific orientation (*i.e.,* the b orientation also known as [010] orientation), the zeolites need to have an anisotropic case. As seen in Figure 39, the MFI zeolites we can synthesize have a disk/coffin shape depending on the size. The smallest dimension is the b-layer. The flats of the zeolites occur on the c-plane and, therefore, these areas have a greater potential to adhere to the surface because of the increased surface area.

[11] We have noticed that the MFI zeolites adhere to the surface better if they are not previously calcined. If the MFI zeolite was calcined prior to the rubbing method, we saw limited or no oriented layer. The mechanism is not completely understood, however, conversations with other zeolite researchers confirmed that we are not the only group to observe this.

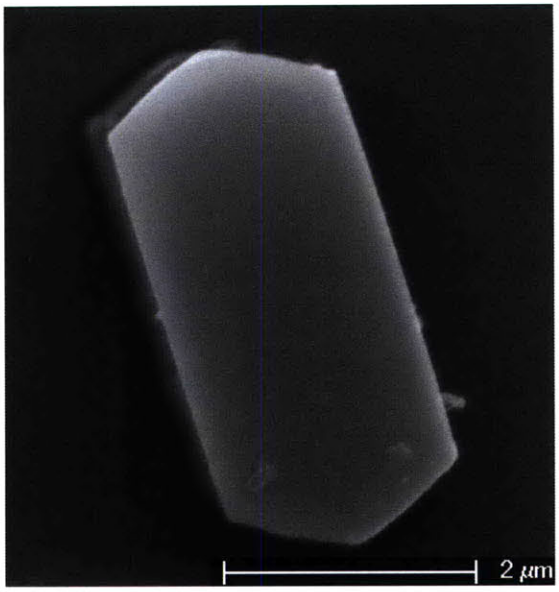

Figure 39. Single MFI zeolite (Si/Al - ∞) synthesized under rotation at 180 C for 12 hours; 5:1:1000 TEOS:TPAOH:H2O.

We fabricated a variety of these zeolites onto a silicon support. Figure 40 shows the range of zeolite sizes that were used, as well as displaying the failure in orienting a monolayer if the size distribution is too large (Figure 40d). The zeolites were oriented directly onto the silicon wafer without an extra adhesion layer of polymer between the zeolite and silicon.

(a)

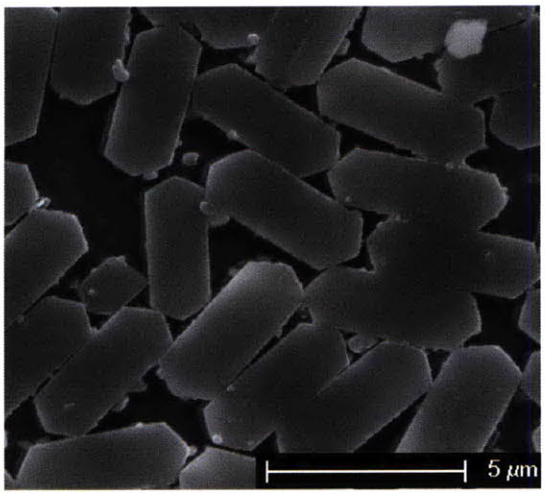

(b)

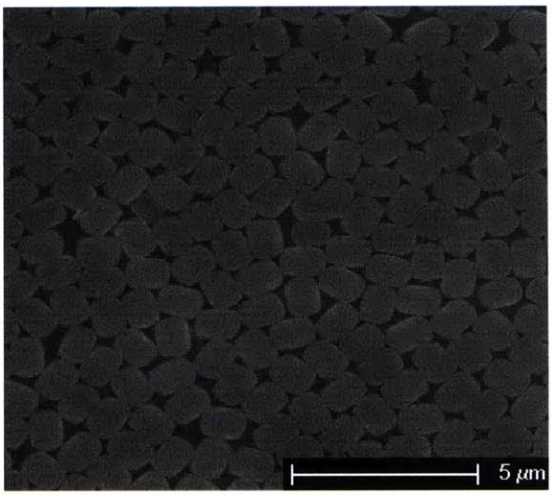

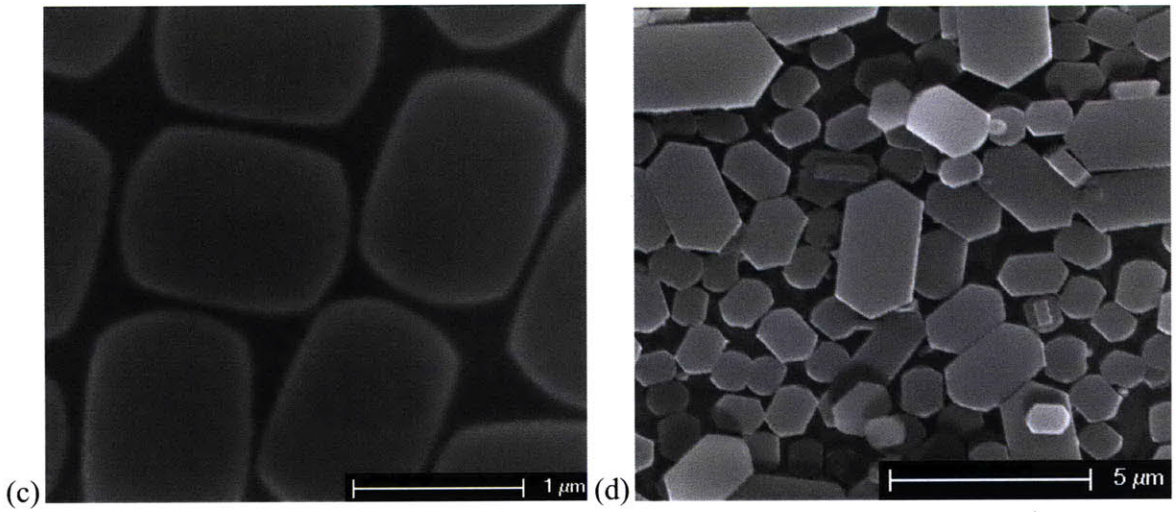

Figure 40 b-oriented MFI zeolite on Si: (a) synthesis conditions: 180°C for 12 hours under rotation (b) 150 °C for 6 hours under rotation (c) 150 °C for 6 hours under rotation (d) 180 °C for 6 hours with no rotation.

We have been able to produce this type of structure on a non-porous silicon wafer, however, we have not been able to reproduce these results on a porous alumina substrate. MFI type zeolites spread and orient easily on a silicon wafer, however, rough porous substrates created unforeseen problems. We attempted to orient the zeolites both with and without an addition polymeric adhesion layer onto a porous alumina support. SEMs are shown in Figure 41. The degree of coverage is very low and the level of orientation is not appropriate for the studies we have planned.

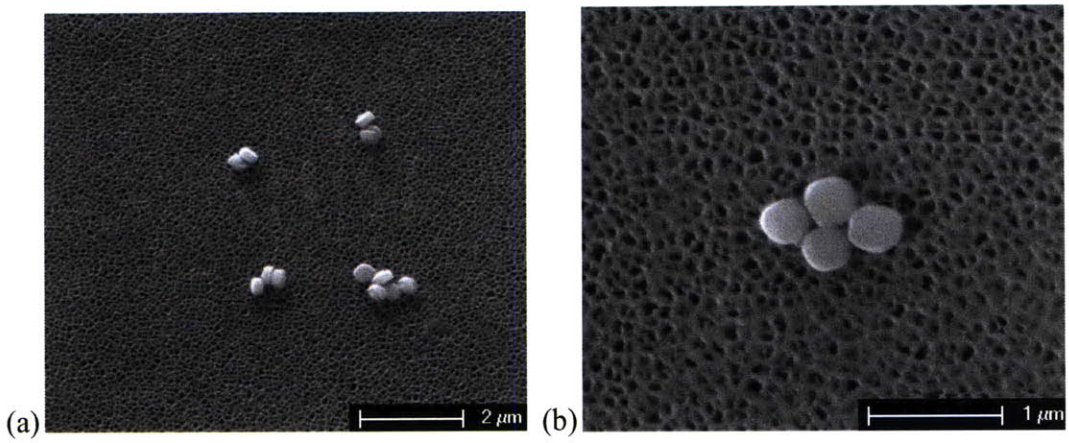

Figure 41. (a) MFI zeolites deposited on a 100 nm Whatman Anodisc functionalized by a PEI adhesion layer. (b) Picture highlighting the low degree of surface coverage with this technique.

We have decided to use a porous glass support (also known as a frit) instead of a porous alumina support. We have been able to orient zeolites onto a glass microscope slide that show the same quality of orientation and coverage as on silicon wafers. We plan on commercially obtaining frits with an average pore size of 1 μm from ROBU ©.

Zeolite orientation and deposition is only one step of the membrane fabrication. A proper material needs to be chosen to fill the gaps between the zeolites. Ideally, the material would be completely impermeable to water and salt. However, in practice, this is difficult to achieve. Solid materials (metals, oxides) can be sputtered or evaporated onto the surface and would be impermeable to any water transport. The difficulty is in filling the gaps between the zeolites because these deposition techniques are line-of-sight and not conformal. Atomic layer deposition (ALD) is an option but the problem is selectively etching the coating that will cover the zeolite surface. Instead of using a metal or an oxide, we decided on using a polymer because of the vast number of methods that polymers can be conformaly coated onto a nanostructure surface and also for the ease of selective removal. We initially attempted to use polyimide for its water-impermeable properties [70]. However, at small length scales (<200 nm), polyimide allows for measurable water and ion transport. It is unclear whether the water was transporting through defects in the thin layer of polyimide or across the medium but, for our applications, we found that it was not sufficient. Instead, we are using divinyl benzene (DVB) that is deposited using an initiated chemical vapor deposition. This step is performed by our collaborators, Prof. Karen Gleason and Rong Yang, at the Institute for Soldier Nanotechnologies at MIT. The thickness of the conformal coating can be controlled from 5 nanometers to a few microns. We tested the permeability of the ions across a 100 nm DVB coating that was deposited on a nanoporous Whatman Anodisc and compared the results to the measured permeabilities of a polyimide coated Anodisc (500 nm coating) and a bare Anodisc. The results show that the DVB suppressed the transport of ions.

To expose the top zeolite surface so that water can enter the pores, the polymer layer must be selectively removed. We use a plasma etch process for this. This type of etch process excites the O_2 or N_2 molecule which then interacts with the surface. For many polymers, such as DVB, the excited molecule will either degrade or displace atoms at the surface. Plasma etching is a mostly line of sight etch and usually cannot expel a molecule if it is confined in a small area. Therefore, the gaps between the zeolites should stay mostly filled with DVB while the surface layer is

etched away. There is a chance that the etch process could affect the surface structure of the zeolite, however, we still need to investigate whether this occurs. A Harrick Plasma © PDC-001 Plasma cleaner with pure oxygen was used to etch a known thickness of DVB deposited on silicon wafer. The change in thickness was determined using a J.A. Woollam Co., spectroscopic ellipsometer. We estimated the etch rate of DVB in 700 microns of O_2 at medium RF power to be 6 nm/min.

5.2 SUMMARY

We outlined the procedure needed to fabricate thin, oriented zeolite membranes for water desalination. The thickness of the membrane is an order of magnitude lower than previous zeolite RO membrane which should lead to an increase in permeability. This method also avoids any secondary growth method, which creates intercrystal pathways around the zeolite for water and salt transport. Challenges associated with producing these membranes onto a porous support exist, however, we are confident that glass supports will be adequate for zeolite orientation. We plan on testing the permeability and salt rejection of the membranes using forward osmosis and electrolytic-driven experiments.

Chapter 6

6. Conclusions and Future Work

In this thesis, we investigated the application of zeolites as an active layer substitute in reverse osmosis membranes for water desalination. Current RO membranes have limited transport that arises from the diffusive transport of water across the non-porous polymeric active layer of the membrane. The permeability could increase if a porous material that is capable of rejecting salt ions while still allowing for water transport replaced this active layer. Although MD simulations have shown that the zeolite pore structure can perfectly reject solvated salt ions while simultaneously allowing for water transport, experimental results have not been able to display the same type of molecular sieving behavior. It is clear that the fundamental mechanisms that govern transport on the sub-nanometer scale of the zeolite pores are not yet clearly understood. By combining studies of the adsorption of water into and on MFI zeolites with the transport of water in the MFI pore structure, we have gained insight into these mechanisms. The confinement of the pore structure combined with the inherent hydrophobicity of the zeolites limits the amount of water that can be adsorbed inside of the zeolite. Past research has shown that water tends to adsorb to the aluminum defect sites; however, these studies have not included the entrance effects of water entering the pore network. We speculate that the entrance effects arise from the strong hydrogen-bonding network of adsorbed water molecules which restricts the diffusion of water molecules into the zeolite pores.

We were able to estimate the amount of adsorbed water in the MFI pore network from the thermogravimetric analysis experiments and corroborate these values with the pressure infiltration studies of water transport into the zeolite pores. Although the two experimental methods are vastly different, the estimate pore volumes for various Si/Al ratio MFI zeolites were found to be approximately the same. The values for the pore volumes filled found by these experiments are ~71-73% for MFI 23 zeolites, ~25-35% for MFI 80 zeolites and 0% for MFI ∞.

The data from these experiments indicates that the Si/Al ratio has a direct effect on the amount of adsorbed water inside the zeolites. Past research has also displayed this trend, however, it was unknown as to how the Si/Al ratio affected the amount of pore volume that was filled. Although we were able to estimate the pore volume that was filled, we have yet to

understand the mobility of the adsorbed water molecules. Determining this mobility is important for determining which mechanism is governing the transport inside of the zeolite pore network.

From the pressure infiltration experiments, we were also able to observe that an increasing volumetric flow rate of water into the zeolite pores had little effect on the infiltration isotherm, an observation that directly contradicts that which is predicted by continuum hydrodynamics. While it is unsurprising that the behavior observed deviated from continuum analysis since the size of the pores was below a nanometer, we do not understand the mechanisms for this type of behavior. It has been seen that water through flowing smooth hydrophobic pores in the nanometer range have exhibited increased slip lengths and flux, so similar mechanisms could be controlling the flow of water in the zeolite pores. Further work to understand this behavior is needed to better understand these mechanisms.

Finally, we have developed a methodology to create defect-free zeolite membranes to test and characterize the water transport and salt rejection properties. Great care must be taken to fabricate these membranes and synthesis parameters must be strictly controlled so that these membranes can be made. We have initiated fabrication of these membranes, but due to challenges in creating membranes on porous supports, the testing has not yet been performed. However, in the future, we anticipate on finishing the fabrication and experimenting on the membranes. From these experiments, we will be able to experimentally demonstrate the possibility that zeolites can act as a molecular sieve for the water desalination process.

6.1 FUTURE WORK

While we have started to understand the mechanisms for the adsorption and transport of water in MFI-type zeolite pores, more experimentation must be performed to fully understand this unique behavior. While decreasing the Si/Al ratio of zeolites also decreases the hydrophobicity, this does not provide any quantitative information about the properties of the adsorbed water in the zeolite pores. The effect of the Al defect sites on the adsorption and, more importantly, the mobility of water in the pores will have a important effect on whether or not zeolites provide any increase in permeability for RO membranes. If the water is strongly adsorbed to the defect sites, permeability through the pores will most likely be low. On the other hand, if there are no defect sites for the water molecules to adsorb to, the pressure infiltration experiments have shown that pressures of 40 MPa and greater are needed to infiltrate the pore

network with water. This pressure is nearly an order of magnitude larger than the average working range that RO facilities operate at. Ideally, there will be some optimal Si/Al ratio where the water adsorbed inside of the zeolite will still be able to transport down the length of the pore and the pressure required to infiltrate the pore network will be minimal. More research is needed to find this optimal value.

To investigate these effects, it is clear that we need to perform our own molecular dynamic simulations in addition to the experiments that we have planned. While past MD simulations have shown promising results, no group has combined the work in order to gain a full understanding of the behavior of water inside of the zeolite pore network. We plan on using the GROMACS software to build the MFI zeolite structure and to study the infiltration and adsorption behavior of varying Si/Al ratio MFI zeolites.

We also plan on expanding our investigation to various other types of zeolites. Murad and Lin looked at the rejection of salt for only one type of pore size. Therefore, it is unclear what the maximum allowable pore size is required so that salt ions are still perfectly rejected. Ideally, we would like the zeolite RO membrane to fully reject the solvated salt ions; however, an increase in the pore diameter should also provide an increase in water permeability. A systematic study of the effect of zeolite pore size on salt rejection should be performed. Not only would it expand on the mechanism of size and salt rejection, but it would also allow researchers to focus on a specific type of zeolite as an RO active layer substitute.

7. Appendix 1

7.1 SILICON/GLASS CLEAN PROCESS

There are various ways to clean a surface, however, we have seen the best results by using a Piranha etch. A Piranha etch is a very strong oxidization solution so, therefore, it will remove nearly all organic material from the surface and it will also hydroxylate the surface. This modifies the surface with OH- (Silanol) groups and thereby makes it extremely hydrophilic. Both of these factors aides in the adhesion of zeolite crystals on the surface.

As a warning, a piranha etch is a **VERY** strong acid solution. It will burn through clothes and skin. Also, if mixed improperly, a piranha etch can explode. Review all appropriate safety training before using this etch.

Chemicals used (used as received):

- 98% H_2SO_4 Sulphuric Acid (Aldrich)
- 100% H_2O_2 Hydrogen Peroxide (Aldrich)

Mix the chemicals by pouring the hydrogen peroxide into the sulphuric acid (never vice versa). To make a 3:1 H_2SO_4:H_2O_2, pour ~30 mL of the sulphuric acid into a Pyrex beaker. Next, slowly (drop by drop) add the hydrogen peroxide. The mixture will become extremely hot. Once the hydrogen peroxide is added, insert the silicon wafers (or glass slides) with PTFE coated tweezers into the beaker and let sit for 3 hours. After three hours, follow appropriate disposal procedures.

7.2 PEI SPIN COATING

If extra adhesion is required (*i.e.,* the zeolites will not adhere to the surface), an extra adhesion layer might be required. We have had the best success with polyetherimine (PEI, Mw = 25,000 g/mol, Sigma). We diluted the PEI with ethanol (Reagent grade,~ 95%, Aldrich). We had the best success with a solution of 1-5 wt% PEI in ethanol. The correct amount of PEI was measured and mixed with the proper amount of ethanol (for example, 1 g of PEI in 20 g of ethanol for a 5 wt% solution). The solution was ultrasonicated for ~30 minutes to create a well dispersed solution. 1 mL of the of the mixed solution was then poured onto a cleaned silicon wafer and placed onto a spin coated. The wafer was then spun at a speed of 3000 RPM for a total time of 1

minute. The wafer was then dried in an oven at 110 °C for 2 hours. At this point, the zeolites could be attached using the manual direct assembly method.

8. Bibliography

1. Shannon, M., et al., *Science and technology for water purification in the coming decades.* Nature, 2008. **452**(7185): p. 301-310.
2. Fritzmann, C., et al., *State-of-the-art of reverse osmosis desalination.* Desalination, 2007. **216**: p. 1-76.
3. Molden, D., International Water Management Institute., and Comprehensive Assessment of Water Management in Agriculture (Program), *Water for food, water for life : a comprehensive assessment of water management in agriculture.* 2007, London ; Sterling, VA: Earthscan. xvii, 645 p.
4. National Research Council (U.S.). Committee on Advancing Desalination Technology. and National Academies Press (U.S.), *Desalination : a national perspective.* 2008, Washington, D.C.: National Academies Press. xiv, 298 p.
5. Wijmans, J. and R. Baker, *The solution-diffusion model: a review*, in *Journal of membrane science.* 1995.
6. Alkhalisi, F.H., *Comparison in Performances of Cellulose-Acetate - Spiral Wound and Polyamide Spiral Wound for Reverse-Osmosis Plant under Iraqi Climate.* Abstracts of Papers of the American Chemical Society, 1988. **195**: p. 212-IEC.
7. Reddy, A.V.R. and P.S. Reddy, *Aromatic Polyamide-Imides as Materials for Membranes .1. Synthesis and Characterization.* Journal of Applied Polymer Science, 1995. **58**(11): p. 1935-1941.
8. Miller, J., *Review of Water Resources and Desalination Technologies.* Sandia National Laboratories Report, SAND2003-0800, 2003.
9. Wright, S.J., J.D. Semrau, and D.R. Keeney, *Microbial Fouling of a Reverse Osmosis Municipal Water Treatment System.* Water Environment Research, 2008. **80**(8): p. 703-707.
10. Liu, L.F., et al., *Study on a novel antifouling polyamide-urea reverse osmosis composite membrane (ICIC-MPD) - III. Analysis of membrane electrical properties.* Journal of membrane science, 2008. **310**(1-2): p. 119-128.
11. Xu, P., et al., *Effect of membrane fouling on transport of organic contaminants in NF/RO membrane applications.* Journal of membrane science, 2006. **279**(1-2): p. 165-175.
12. Feng, D., J.S.J. van Deventer, and C. Aldrich, *Ultrasonic defouling of reverse osmosis membranes used to treat wastewater effluents.* Separation and Purification Technology, 2006. **50**(3): p. 318-323.
13. Madaeni, S.S. and Y. Mansourpanah, *Chemical cleaning of reverse osmosis membranes fouled by whey.* Desalination, 2004. **161**(1): p. 13-24.
14. Fornasiero, F., et al., *Ion exclusion by sub-2-nm carbon nanotube pores.* Proceedings of the National Academy of Sciences, 2008. **105**(45): p. 17250-17250.
15. Holt, J.K., et al., *Fast mass transport through sub-2-nanometer carbon nanotubes.* Science, 2006. **312**(5776): p. 1034-1037.
16. Murata, K., et al., *Structural determinants of water permeation through aquaporin-1.* Nature, 2000. **407**: p. 599-605.

17. Zuo, G., et al., *Transport Properties of Single-File Water Molecules inside a Carbon Nanotube Biomimicking Water Channel.* ACS Nano, 2010. **4**(1): p. 205-210.
18. Gong, X., et al., *A charge-driven molecular water pump.* Nature nanotechnology, 2007. **2**: p. 709-712.
19. Fornasiero, F., et al., *Ion exclusion by sub-2-nm carbon nanotube pores*, in *Proceedings of the National Academy of Sciences*. 2008. p. 17250.
20. Nightingale Jr, E., *Phenomenological theory of ion solvation. Effective radii of hydrated ions.* The Journal of Physical Chemistry, 1959. **63**(9): p. 1381-1387.
21. Cejka, J., *Introduction to zeolite science and practice.* 2007: p. 1-1058.
22. OLSON, D., et al., *CRYSTAL-STRUCTURE AND STRUCTURE-RELATED PROPERTIES OF ZSM-5.* J Phys Chem-Us, 1981. **85**(15): p. 2238-2243.
23. Israelachvili, J.N., *Intermolecular and surface forces*. 2nd ed. 1991, London ; San Diego: Academic Press. xxi, 450 p.
24. Koros, W.J. and R. Mahajan, *Pushing the limits on possibilities for large scale gas separation: which strategies?* Journal of membrane science, 2001. **181**(1): p. 141-141.
25. Tomita, T., K. Nakayama, and H. Sakai, *Gas separation characteristics of DDR type zeolite membrane.* Microporous and Mesoporous Materials, 2004. **68**(1-3): p. 71-75.
26. Gur, T.M., *Permselectivity of Zeolite Filled Polysulfone Gas Separation Membranes.* Journal of membrane science, 1994. **93**(3): p. 283-289.
27. Murad, S.M. and J.C. Lin, *Using Thin Zeolite Membranes and External Electric Fields To Separate Supercritical Aqueous Electrolyte Solutions.* Ind. Eng. Chem. Res, 2002. **41**: p. 1076-1083.
28. Li, L., et al., *Desalination by reverse osmosis using MFI zeolite membranes.* Journal of membrane science, 2004. **243**: p. 401-404.
29. Lai, Z., M. Tsapatsis, and J.P. Nicolich, *Siliceous ZSM-5 Membranes by Secondary Growth of b-Oriented Seed Layers.* Advanced Functional Materials, 2004. **14**(7): p. 716-729.
30. Jeong, B., et al., *Interfacial polymerization of thin film nanocomposites: A new concept for reverse osmosis membranes*, in *Journal of Membrane Science*. 2007. p. 1-7.
31. Barrer, R.M., *Factors Governing the Growth of Crystalline Silicates.* Discussions of the Faraday Society, 1949(5): p. 326-339.
32. Wang, J., et al., *Facile synthesis of ZSM-5 composites with hierarchical porosity.* Journal of Materials Chemistry, 2008. **18**.
33. Van Koningsveld, H., H. Van Bekkum, and J. Jansen, *On the location and disorder of the tetrapropylammonium (TPA) ion in zeolite ZSM-5 with improved framework accuracy.* Acta Crystallographica Section B: Structural Science, 1987. **43**(2): p. 127-132.
34. *XRD Theory*. [cited 2010 August 4]; Available from: http://www.ksanalytical.com/theory/.
35. Zachariasen, W.H., *Theory of X-ray diffraction in crystals*. 1967, New York,: Dover Publications. vii, 255 p.
36. Carvalho, L.C.d., *XPS Analysis*, XPSsystem.gif, Editor. 2009.
37. Rouquerol, F., J. Rouquerol, and K.S.W. Sing, *Adsorption by powders & porous solids : principles, methodology and applications*. 1999, San Diego, Calif.: Academic Press. xvi, 467 p.
38. Flanigen, E.M., et al., *Silicalite, a New Hydrophobic Crystalline Silica Molecular-Sieve.* Nature, 1978. **271**(5645): p. 512-516.
39. Schroder, J., *Characterization of Porous Solids.* Chemie Ingenieur Technik, 1988. **60**(2): p. 152-153.

40. Sing, K.S.W., *Characterization of Porous Solids* Characterization of Porous Solids Ii, 1991. **62**: p. 1-782.
41. Brunauer, S., P.H. Emmett, and E. Teller, *Adsorption of gases in multimolecular layers.* Journal of the American Chemical Society, 1938. **60**: p. 309-319.
42. Kenny, M.B. and K.S.W. Sing, *The Hydrophobicity of Silicalite and Zsm-5.* Chemistry & Industry, 1990(2): p. 39-40.
43. Chen, N.Y., *Hydrophobic Properties of Zeolites.* Journal of Physical Chemistry, 1976. **80**(1): p. 60-64.
44. Hill, S.G. and D. Seddon, *The Hygroscopic Nature of H-Zsm-5.* Zeolites, 1985. **5**(3): p. 173-178.
45. Jentys, A., et al., *Adsorption of Water on Zsm5 Zeolites.* Journal of Physical Chemistry, 1989. **93**(12): p. 4837-4843.
46. Callister, W.D. and D.G. Rethwisch, *Materials science and engineering : an introduction.* 8th ed. 2010, Hoboken, NJ: John Wiley & Sons. xxiii, 885, [82] p.
47. Ari, M.U., et al., *Molecular Dynamics Simulation of Water Diffusion in MFI-Type Zeolites.* Journal of Physical Chemistry B, 2009. **113**(23): p. 8073-8079.
48. Fleys, M., R.W. Thompson, and J.C. MacDonald, *Comparison of the behavior of water in silicalite and dealuminated zeolite Y at different temperatures by molecular dynamic simulations.* Journal of Physical Chemistry B, 2004. **108**(32): p. 12197-12203.
49. Bussai, C., et al., *On the diffusion of water in silicalite-1: MD simulations using ab initio fitted potential and PFG NMR measurements.* Applied Catalysis a-General, 2002. **232**(1-2): p. 59-66.
50. Demontis, P., G. Stara, and G.B. Suffritti, *Behavior of water in the hydrophobic zeolite silicalite at different temperatures. A Molecular Dynamics Study.* Journal of Physical Chemistry B, 2003. **107**(18): p. 4426-4436.
51. Han, A. and Y. Qiao, *Infiltration of liquid water in an acid-leached zeolite.* Journal of Materials Research, 2007. **22**(12): p. 3538-3541.
52. Qiao, Y., L. Liu, and X. Chen, *Pressurized Liquid in Nanopores: A Modified Laplace-Young Equation*, in *Nano Lett.* 2009.
53. Zhao, J., et al., *Experimental Study on Energy Dissipation of Electrolytes in Nanopores.* Langmuir, 2009. **25**(21): p. 12687–12696.
54. Joseph, S. and N.R. Aluru, *Why are carbon nanotubes fast transporters of water?* Nano Letters, 2008. **8**(2): p. 452-458.
55. Eroshenko, V., et al., *Energetics: a new field of applications for hydrophobic zeolites*, in *J. Am. Chem. Soc.* 2001. p. 8129-8130.
56. Liu, L., Y. Qiao, and X. Chen, *Pressure-driven water infiltration into carbon nanotube.* Applied Physics Letters, 2008. **92**(101927): p. 1-3.
57. Han, A. and Y. Qiao, *Influence of surface treatment on defiltration of confined liquid in MCM-41*, in *Chemical Physics Letters.* 2008.
58. Han, A. and Y. Qiao, *Infiltration of liquid water in an acid-leached zeolite*, in *Journal of Materials Research.* 2007.
59. Kim, T., et al., *Effects of anion concentration on ion-transport pressure in nanopores.* Appl Phys Lett, 2009. **94**(1): p. 013105.
60. Trzpit, M., et al., *The effect of local defects on water adsorption in silicalite-1 zeolite: a joint experimental and molecular simulation study.* Langmuir: the ACS journal of surfaces and colloids, 2007. **23**(20): p. 10131.

61. Trzpit, M., M. Soulard, and J. Patarin, *Water intrusion in mesoporous silicalite-1: An increase of the stored energy.* Microporous and Mesoporous Materials, 2009. **117**(3): p. 627-634.
62. Cailliez, F., et al., *Thermodynamics of water intrusion in nanoporous hydrophobic solids.* Phys Chem Chem Phys, 2008. **10**(32): p. 4817-4826.
63. Qiao, Y., L. Liu, and X. Chen, *Pressurized Liquid in Nanopores: A Modified Laplace-Young Equation.* Nano Lett, 2009. **9**(3): p. 984-988.
64. Wan, Y.S.S., et al., *Design and fabrication of zeolite-based microreactors and membrane microseparators.* Microporous and Mesoporous Materials, 2001. **42**(2-3): p. 157-175.
65. Choi, J., et al., *MFI zeolite membranes from a- and randomly oriented monolayers.* Adsorption-Journal of the International Adsorption Society, 2006. **12**(5-6): p. 339-360.
66. Xomeritakis, G., S. Nair, and M. Tsapatsis, *Transport properties of alumina-supported MFI membranes made by secondary (seeded) growth.* Microporous and Mesoporous Materials, 2000. **38**(1): p. 61-73.
67. Li, L., et al., *Reverse osmosis through MFI zeolite membranes: implications for produced water desalination.* Desalination, 2008(18300432218665337715related:c0OpnSQy-P0J).
68. Lee, J.S., et al., *Manual assembly of microcrystal monolayers on substrates.* Angew Chem Int Edit, 2007. **46**(17): p. 3087-3090.
69. Liu, Y., Y. Li, and W. Yang, *Fabrication of highly b-oriented MFI monolayers on various substrates.* Chemical Communications, 2009.
70. Matsuura, T., et al., *Polyimide Derived from 2,2'-Bis(Trifluoromethyl)-4,4'-Diaminobiphenyl .1. Synthesis and Characterization of Polyimides Prepared with 2,2-Bis(3,4-Dicarboxyphenyl)Hexafluoropropane Dianhydride or Pyromellitic Dianhydride.* Macromolecules, 1991. **24**(18): p. 5001-5005.